



Discontinuous Galerkin methods for short pulse type equations via hodograph transformations

Qian Zhang, Yinhua Xia^{*,1}

School of Mathematical Sciences, University of Science and Technology of China, Hefei, Anhui 230026, PR China



ARTICLE INFO

Article history:

Received 9 January 2019

Received in revised form 19 August 2019

Accepted 3 September 2019

Available online 11 September 2019

Keywords:

Discontinuous Galerkin method

Short pulse equation

Nonclassical soliton solution

Conservative scheme

Hodograph transformation

ABSTRACT

In the present paper, we consider the discontinuous Galerkin (DG) methods for solving short pulse (SP) type equations. The short pulse equation has been shown to be completely integrable, which admits the loop-soliton, cuspon-soliton solutions as well as smooth-soliton solutions. Through hodograph transformations, these nonclassical solutions can be profiled as the smooth solutions of the coupled dispersionless (CD) system or the sine-Gordon equation. Therefore, DG methods can be developed for the CD system or the sine-Gordon equation to simulate the loop-soliton or cuspon-soliton solutions of the SP equation. The conservativeness or dissipation of the Hamiltonian or momentum for the semi-discrete DG schemes can be proved. Also we modify the above DG schemes and obtain an integration DG scheme. Theoretically the a-priori error estimates have been provided for the momentum conserved DG scheme and the integration DG scheme. We also propose the DG scheme and the integration DG scheme for the sine-Gordon equation, in case the SP equation can not be transformed to the CD system. All these DG schemes can be applied to the generalized or modified SP type equations. Numerical experiments are provided to illustrate the optimal order of accuracy and capability of these DG schemes.

© 2019 Elsevier Inc. All rights reserved.

1. Introduction

In this paper, we mainly study the classic short pulse (SP) equation derived by Schäfer and Wayne in [27]

$$u_{xt} = u + \frac{1}{6}(u^3)_{xx}. \quad (1.1)$$

The SP equation models the propagation of ultra-short light pulses in silica optical fibers. Here, $u \in \mathbb{R}$ is a real-valued function which represents the magnitude of the electric field. It is well-known that the cubic nonlinear Schrödinger (NLS) equation derived from the Maxwell's equation can describe the propagation of pulse in optical fibers. Two preconditions of this derivation need to be satisfied: First, the response of the material attains a quasi-steady-state and second that the pulse width is as large as the oscillation of the carrier frequency. And now we can create very short pulses by the advanced technology and the pulse spectrum is not narrowly localized around the carrier frequency, that is, when the pulse is as short as a few cycles of the central frequency. Numerical experiments made in [8] show as the pulse shortens, the accuracy of the SP equation approximated to Maxwell's equation increases, however, the NLS equation becomes inaccurate for the

* Corresponding author.

E-mail addresses: gelee@mail.ustc.edu.cn (Q. Zhang), yhxia@ustc.edu.cn (Y. Xia).

¹ Research supported by NSFC grant No. 11871449, and a grant from Laboratory of Computational Physics (No. 6142A0502020817).

ultra-short pulse. Therefore, we use SP equation to approximate the ultra-short light pulse. If the pulse is as short as only one cycle of its carrier frequency, then the modified short pulse equation in [30] is used to describe the propagation of pulse in optical fibers. Similar to the extension of coupled nonlinear Schrödinger equations from NLS equations, it is necessary to consider its two-component or multi-component generalizations for describing the effect of polarization or anisotropy [10,24,31]. For birefringent fibers, the authors in [11,14] also introduced some extensions of the SP equation to describe the propagation of ultra-short pulse. We will introduce these extensions specifically in Section 3.

Integrable discretizations of short pulse type equations have received considerable attention recently, especially the loop-soliton, antiloop-soliton and cuspon-soliton solutions in [11,13,14,12,31]. The authors linked the short pulse type equations with the coupled dispersionless (CD) type systems or the sine-Gordon type equations through the hodograph transformations. The key of the discretization is an introduction of a nonuniform mesh, which plays a role of the hodograph transformations as in continuous case. In this paper, we aim at solving the loop-soliton, cuspon-soliton solutions of the short pulse type equations as well as smooth-soliton solutions. Through the hodograph transformation $(x, t) \rightarrow (y, s)$ which was proposed in [28],

$$\begin{cases} \frac{\partial}{\partial x} = \frac{1}{\rho} \frac{\partial}{\partial y}, \\ \frac{\partial}{\partial t} = \frac{\partial}{\partial s} + \frac{u^2}{2\rho} \frac{\partial}{\partial y}, \end{cases}$$

we can establish the link between the SP equation (1.1) and the CD system [19],

$$\rho_s + \left(\frac{1}{2}u^2\right)_y = 0, \quad u_{ys} = \rho u.$$

There exists some short pulse type equations which are failed to be transformed into CD systems. Therefore, we consider an alternative approach by introducing a new variable z and define another hodograph transformation,

$$\begin{cases} \frac{\partial}{\partial x} = (\cos z)^{-1} \frac{\partial}{\partial y}, \\ \frac{\partial}{\partial t} = \frac{\partial}{\partial s} + \frac{1}{2}z_s^2 (\cos z)^{-1} \frac{\partial}{\partial y}, \end{cases}$$

which connects the short pulse equation (1.1) with the sine-Gordon equation [30]

$$z_{ys} = \sin z.$$

For the CD system or the sine-Gordon equation, we develop the discontinuous Galerkin (DG) schemes to obtain the high-order accuracy numerical solution $u_h(y, s)$ or $z_h(y, s)$. Consequently, a point-to-point profile $u_h(x, t)$ of loop-soliton, cuspon-soliton solutions of the SP equation can be obtained, which are shown by the numerical experiments in Section 4.

The DG method was first introduced in 1973 by Reed and Hill in [26] for solving steady state linear hyperbolic equations. The important ingredient of this method is the design of suitable inter-element boundary treatments (so called numerical fluxes) to obtain highly accurate and stable schemes in many situations. Within the DG framework, the method was extended to deal with derivatives of order higher than one, i.e. local discontinuous Galerkin (LDG) method. The first LDG method was introduced by Cockburn and Shu in [7] for solving convection-diffusion equation. Their work was motivated by the successful numerical experiments of Bassi and Rebay [2] for compressible Navier-Stokes equations. Later, Yan and Shu developed an LDG method for a general KdV type equation containing third order derivatives in [42], and they generalized the LDG method to PDEs with fourth and fifth spatial derivatives in [43]. Levy, Shu and Yan [21] developed LDG methods for nonlinear dispersive equations that have compactly supported traveling wave solutions, the so-called compactons. More recently, Xu and Shu further generalized the LDG method to solve a series of nonlinear wave equations [37–40,45]. We refer to the review paper [36] of LDG methods for high-order time-dependent partial differential equations.

Most recently, a series of schemes which called structure-preserving schemes have attracted considerable attention. For some integrable equations like KdV type equations [9,20,22,46], Zakharov system [34], Schrödinger-KdV system [35], Camassa-Holm equation [44], etc., the authors proposed various conservative numerical schemes to “preserve structure”. These conservative numerical schemes have some advantages over the dissipative ones, for example, the Hamiltonian conservativeness can help reduce the phase error along the long time evolution and have a more accurate approximation to exact solutions for KdV type equations [46]. The CD system and the generalized CD system are integrable, thus they have an infinite number of conserved quantities [18]. For the CD system, the following two invariants

$$H_0 = \int \rho u^2 dy, \quad H_1 = \int \rho^2 + u_y^2 dy,$$

are corresponding to the Hamiltonian E_0, E_1 of the SP equation [3,4] via the hodograph transformation,

$$E_0 = \int u^2 dx, \quad E_1 = \int \sqrt{1 + u_x^2} dx.$$

In this paper, we first construct E_0 conserved DG scheme for the SP equation directly. For the loop-soliton and cuspon-soliton solutions, the H_0, H_1 conserved DG schemes for CD system are developed respectively, to profile the singular

solutions of the SP equation. Also we modify the above DG schemes and propose an integration DG scheme which can numerically achieve the optimal convergence rates for ρ, u , and u_y . Theoretically, we prove that the H_1 conserved DG scheme has the optimal order of accuracy for ρ, u and u_y in L^2 norm. The integration DG scheme can be proved the optimal order of accuracy for ρ, u_y in L^2 norm and the suboptimal order of accuracy for u in L^∞ norm. All these DG schemes can be adopted to the generalized or modified SP type equations.

The rest of this paper is organized as follows. In Section 2, we develop the DG schemes for the SP equation directly, and via the hodograph transformations for the CD system and the sine-Gordon equation. Some notations for simplifying expressions are given in Section 2.1. In Section 2.2, we first propose the E_0 conserved DG scheme for the SP equation. To simulate the loop-soliton or cuspon-soliton solutions of the SP equation, the H_0, H_1 conserved DG schemes and the integration DG scheme are constructed for the CD system which links the SP equation by the hodograph transformation. Meanwhile, the a priori error estimates for H_1 conserved DG and integration DG schemes are also provided. Moreover, we develop two kinds of DG schemes for the sine-Gordon equation to introduce another resolution for the SP equation in Section 2.3. Section 3 is devoted to summarize the generalized short pulse equations and introduce the corresponding conserved quantities briefly. Several numerical experiments are listed in Section 4, including the propagation and interaction of loop-soliton, cuspon-solution, breather solution of the short pulse type equations. We also show the accuracy and the change of conserved quantities in Section 4. Finally, some concluding remarks are given in Section 5.

2. The discontinuous Galerkin discretization

In this section, we present the discontinuous Galerkin discretization for solving the short pulse type equations. In order to describe the methods, we first introduce some notations.

2.1. Notations

We denote the mesh \mathcal{T}_h on the spatial y by $I_j = [y_{j-\frac{1}{2}}, y_{j+\frac{1}{2}}]$ for $j = 1, \dots, N$, with the cell center denoted by $y_j = \frac{1}{2}(y_{j-\frac{1}{2}} + y_{j+\frac{1}{2}})$. The cell size is $\Delta y_j = y_{j+\frac{1}{2}} - y_{j-\frac{1}{2}}$ and $h = \max_{1 \leq j \leq N} \Delta y_j$. The mesh is regular in the sense that the ratio between the maximum and the minimum mesh sizes stays bounded during mesh refinements. The finite element space as the solution and test function space consists of piecewise polynomials

$$V_h^k = \{v : v|_{I_j} \in P^k(I_j); 1 \leq j \leq N\},$$

where $P^k(I_j)$ denotes the set of polynomial of degree up to k defined on the cell I_j . Notably, the functions in V_h^k are allowed to be discontinuous across cell interfaces. The values of u at $y_{j+\frac{1}{2}}$ are denoted by the $u_{j+\frac{1}{2}}^-$ and $u_{j+\frac{1}{2}}^+$, from the left cell I_j and the right cell I_{j+1} respectively. Additionally, the jump of u is defined as $\llbracket u \rrbracket = u^+ - u^-$, the average of u as $\{u\} = \frac{1}{2}(u^+ + u^-)$. To simplify expressions, we adopt the round bracket and angle bracket for the L^2 inner product on cell I_j and its boundary

$$(u, v)_{I_j} = \int_{I_j} uv dy,$$

$$\langle \hat{u}, v \rangle_{I_j} = \hat{u}_{j+\frac{1}{2}} v_{j+\frac{1}{2}}^- - \hat{u}_{j-\frac{1}{2}} v_{j-\frac{1}{2}}^+,$$

for one dimensional case.

For the spatial variable x , we denote the mesh \mathcal{T}_h' by $I_j' = [x_{j-\frac{1}{2}}, x_{j+\frac{1}{2}}]$ for $j = 1, \dots, N$. Similar to the notations on the mesh \mathcal{T}_h , we have $x_j, \Delta x_j$, and $h' = \max_{1 \leq j \leq N} \Delta x_j$. We assume that the mesh on the coordinate x is also regular. Without misunderstanding, we still use $u_{j+\frac{1}{2}}^-$ and $u_{j+\frac{1}{2}}^+$ denote the values of u at $x_{j+\frac{1}{2}}$, from the left cell I_j' and the right cell I_{j+1}' respectively.

2.2. The short pulse equation

Recall the short pulse equation

$$u_{xt} = u + \frac{1}{6}(u^3)_{xx}, \quad x \in I' = [x_L, x_R], \quad (2.1)$$

where $u(x, t) \in \mathbb{R}$ is a real-valued function, t denotes the temporal coordinate and x is the spatial scale. Through the hodograph transformation, it can be converted into a coupled dispersionless (CD) system

$$\begin{cases} \rho_s + (\frac{1}{2}u^2)_y = 0, \\ u_{ys} = \rho u, \end{cases} \quad (2.2)$$

where s denotes the temporal coordinate, and y is the spatial scale, $y \in I = [y_L, y_R]$. The hodograph transformation $(y, s) \rightarrow (x, t)$ is defined by

$$\begin{cases} \frac{\partial}{\partial y} = \rho \frac{\partial}{\partial x}, \\ \frac{\partial}{\partial s} = \frac{\partial}{\partial t} - \frac{u^2}{2} \frac{\partial}{\partial x}. \end{cases}$$

Subsequently, the parametric representation of the solution of the short pulse equation (2.1) is

$$u = u(y, s), \quad x = x(y_0, s) + \int_{y_0}^y \rho(\zeta, s) d\zeta,$$

where y_0 is a real constant. Since the short pulse equation and the equivalent CD system are completely integrable, they have an infinite number of conservation laws. The first two invariants of the SP equation are described by

$$E_0 = \int u^2 dx, \quad E_1 = \int \sqrt{1 + u_x^2} dx,$$

and the corresponding conservation laws for the CD system are

$$H_0 = \int \rho u^2 dy, \quad H_1 = \int \rho^2 + u_y^2 dy.$$

2.2.1. E_0 conserved scheme

To construct the discontinuous Galerkin method for the SP equation directly, we rewrite the SP equation (2.1) as a first order system:

$$\begin{cases} v_t = u + \omega_x, \\ v = u_x, \\ \omega = (\frac{1}{6}u^3)_x. \end{cases} \quad (2.3)$$

The local DG scheme for equations (2.3) is formulated as follows: Find $u_h, v_h, \omega_h \in V_h^k$ such that, for all test functions $\varphi, \phi, \psi \in V_h^k$ and $I'_j \in \mathcal{T}'_h$

$$\begin{cases} ((v_h)_t, \varphi)_{I'_j} = (u_h, \varphi)_{I'_j} + \langle \widehat{\omega_h}, \varphi \rangle_{I'_j} - (\omega_h, \varphi_x)_{I'_j}, & (a) \\ (v_h, \phi)_{I'_j} = \langle \widehat{u_h}, \phi \rangle_{I'_j} - (u_h, \phi_x)_{I'_j}, & (b) \\ (\omega_h, \psi)_{I'_j} = \langle \widehat{f(u_h)}, \psi \rangle_{I'_j} - (f(u_h), \psi_x)_{I'_j}, & (c) \end{cases} \quad (2.4)$$

where $f(u) = \frac{1}{6}u^3$. The “hat” terms in the scheme are the so-called “numerical fluxes”, which are functions defined on the cell boundary from integration by parts and should be designed based on different guiding principles for different PDEs to ensure the stability and local solvability of the intermediate variables. To ensure the scheme is E_0 conserved, the numerical fluxes we take are

$$\begin{cases} \widehat{\omega_h} = \{\omega_h\}, \quad \widehat{u_h} = \{u_h\}, \\ \widehat{f(u)} = \begin{cases} \frac{\llbracket F(u) \rrbracket}{\llbracket u \rrbracket}, & \llbracket u \rrbracket \neq 0, \\ f(\llbracket u \rrbracket), & \llbracket u \rrbracket = 0, \end{cases} \end{cases} \quad (2.5)$$

where $F(u) = \int^u f(\tau) d\tau$. Numerically, E_0 conserved DG scheme can achieve $(k+1)$ -th order of accuracy for even k , and k -th order of accuracy for odd k on uniform meshes. With nonuniform meshes, the E_0 conserved DG scheme only have suboptimal order of accuracy regardless of the parity of the polynomial degrees k .

Proposition 2.1. (Energy conservation) The DG scheme (2.4) with the numerical fluxes (2.5) for the short pulse equation (2.1) satisfies the energy conservativeness

$$\frac{d}{dt} E_0(u_h) = 0.$$

Proof. For the equation (2.4b), we take the time derivative and get

$$((v_h)_t, \eta)_{I'_j} = \langle \widehat{(u_h)_t}, \eta \rangle_{I'_j} - ((u_h)_t, \eta_x)_{I'_j}. \quad (2.6)$$

Since (2.6), and (2.4a)-(2.4c) hold for any test functions in V_h^k , we can choose

$$\varphi = (u_h)_t, \quad \eta = -(u_h)_t, \quad \psi = -u_h,$$

and it follows that

$$((v_h)_t, (u_h)_t)_{I'_j} = (u_h, (u_h)_t)_{I'_j} + \langle \widehat{\omega_h}, (u_h)_t \rangle_{I'_j} - (\omega_h, (u_h)_{tx})_{I'_j}, \quad (2.7)$$

$$-((v_h)_t, (u_h)_t)_{I'_j} = -\langle \widehat{(u_h)_t}, (u_h)_t \rangle_{I'_j} + ((u_h)_t, (u_h)_{tx})_{I'_j}, \quad (2.8)$$

$$-(\omega_h, u_h)_{I'_j} = -\langle \widehat{f(u_h)}, (u_h) \rangle_{I'_j} + (f(u_h), (u_h)_x)_{I'_j}. \quad (2.9)$$

To eliminate extra terms, we take test functions $\varphi = -\omega_h$ in (2.4a), $\eta = \omega_h$ in (2.6), and then obtain

$$-((v_h)_t, \omega_h)_{I'_j} = -(u_h, \omega_h)_{I'_j} - \langle \widehat{\omega_h}, \omega_h \rangle_{I'_j} + (\omega_h, (\omega_h)_x)_{I'_j}, \quad (2.10)$$

$$((v_h)_t, \omega_h)_{I'_j} = \langle \widehat{(u_h)_t}, \omega_h \rangle_{I'_j} - ((u_h)_t, (\omega_h)_x)_{I'_j}. \quad (2.11)$$

With these choices of test functions and summing up the five equations in (2.7)-(2.11), we get

$$\begin{aligned} (u_h, (u_h)_t)_{I'_j} + \langle \widehat{\omega_h}, (u_h)_t \rangle_{I'_j} - (\omega_h, (u_h)_{tx})_{I'_j} - \langle \widehat{(u_h)_t}, (u_h)_t \rangle_{I'_j} + ((u_h)_t, (u_h)_{tx})_{I'_j} \\ + \langle \widehat{(u_h)_t}, \omega_h \rangle_{I'_j} - ((u_h)_t, (\omega_h)_x)_{I'_j} - \langle \widehat{f(u_h)}, (u_h) \rangle_{I'_j} + (f(u_h), (u_h)_x)_{I'_j} \\ - \langle \widehat{\omega_h}, \omega_h \rangle_{I'_j} + (\omega_h, (\omega_h)_x)_{I'_j} = 0. \end{aligned} \quad (2.12)$$

Now the equation (2.12) can be rewritten into following form

$$(u_h, (u_h)_t)_{I'_j} + \Phi_{j+\frac{1}{2}} - \Phi_{j-\frac{1}{2}} + \Theta_{j-\frac{1}{2}} = 0, \quad (2.13)$$

where the numerical entropy flux Φ is given by

$$\begin{aligned} \Phi = \widehat{\omega_h}(u_h^-)_t - \omega_h^-(u_h^-)_t + \frac{1}{2}(u_h^-)_t^2 - \widehat{(u_h)_t}(u_h^-)_t \\ + \widehat{(u_h)_t}\omega_h^- - \frac{1}{2}(\omega_h^-)^2 + \widehat{\omega_h}\omega_h^- - \widehat{f(u_h)}u_h^- + F(u_h^-), \end{aligned}$$

and the extra term Θ is

$$\begin{aligned} \Theta = -\widehat{\omega_h}[\![u_h]_t\!] - \widehat{(u_h)_t}[\![w_h]\!] + [\![w_h(u_h)_t]\!] + \widehat{f(u_h)}[\![u_h]\!] - [\![F(u_h)]\!] \\ + \widehat{(u_h)_t} - [\![u_h]_t\!]\}[\![u_h]_t\!] + (-\widehat{\omega_h} + [\![\omega_h]\!])[\![\omega_h]\!] = 0, \end{aligned}$$

which vanishes due to the choice of the conservative numerical fluxes (2.5). Summing up the cell entropy equalities (2.13) with the periodic or homogeneous Dirichlet boundary conditions, it implies that

$$(u_h, (u_h)_t)_{I'} = 0.$$

Thus, the DG scheme (2.4) for the short pulse equation is E_0 conserved. \square

The E_0 conserved scheme resolves the smooth solutions for the short pulse equation efficiently, as shown in Section 4. However, for the loop-soliton and cuspon-soliton solutions, this scheme can not be used because of the singularity of solutions. Therefore, we introduce the DG schemes via hodograph transformations in the following sections.

2.2.2. H_0 conserved DG scheme

As we have mentioned, the short pulse equation can be converted into the coupled dispersionless (CD) system through the hodograph transformation. To construct the local discontinuous Galerkin numerical method for the CD system, we first rewrite (2.2) as a first order system

$$\begin{cases} \rho_s + \gamma_y = 0, \\ \omega_s = \rho u, \\ \omega = u_y, \\ \gamma = \frac{1}{2}u^2. \end{cases}$$

Then we can formulate the LDG numerical method as follows: Find $u_h, \rho_h, \omega_h, \gamma_h \in V_h^k$ such that

$$\begin{cases} ((\rho_h)_s, \phi)_{I_j} + \langle \widehat{\gamma}_h, \phi \rangle_{I_j} - (\gamma_h, \phi_y)_{I_j} = 0, & (a) \\ ((\omega_h)_s, \varphi)_{I_j} = (\rho_h u_h, \varphi)_{I_j}, & (b) \\ (\omega_h, \psi)_{I_j} = \langle \widehat{u}_h, \psi \rangle_{I_j} - (u_h, \psi_y)_{I_j}, & (c) \\ (\gamma_h, \eta)_{I_j} = (\frac{1}{2} u_h^2, \eta)_{I_j} & (d) \end{cases} \quad (2.14)$$

for all test functions $\phi, \varphi, \psi, \eta \in V_h^k$ and $I_j \in \mathcal{T}_h$. To guarantee the conservativeness of H_0 , we adopt the central numerical fluxes

$$\widehat{\gamma}_h = \{\{\gamma_h\}\}, \quad \widehat{u}_h = \{\{u_h\}\}. \quad (2.15)$$

Here, the Dirichlet boundary condition is imposed. Numerically, on uniform meshes, we will see that the optimal $(k+1)$ -th order of accuracy can be obtained for u_h, ρ_h when k is even, however, the numerical solutions u_h, ρ_h have k -th order of accuracy when k is odd. If we modify numerical fluxes as below:

$$\widehat{\gamma}_h = \{\{\gamma_h\}\} - \alpha \llbracket \rho_h \rrbracket - \beta \llbracket \gamma_h \rrbracket, \quad \widehat{u}_h = \{\{u_h\}\} + \mu \llbracket u_h \rrbracket, \quad (2.16)$$

then the scheme is dissipative on H_0 with the appropriate parameters in Proposition 2.2 and the optimal order of accuracy can be achieved numerically for this H_0 dissipative scheme.

Proposition 2.2. (H_0 conservation/dissipation) *The semi-discrete DG numerical scheme (2.14), (2.15) can preserve quantity $H_0(\rho_h, u_h) = \int_I \rho_h u_h^2 dy$ spatially. The scheme (2.14) with (2.16) composes a dissipative DG scheme on H_0 if the parameters in (2.16) satisfy the conditions*

$$\alpha = 0, \quad \beta \geq 0, \quad \mu \geq 0 \text{ and } \beta + \mu \neq 0.$$

Proof. First, we take time derivative of equation (2.14c), and the test functions are chosen as $\phi = \gamma_h, \varphi = -(u_h)_s, \psi = (u_h)_s, \eta = -(\rho_h)_s$. Then we have

$$((\rho_h)_s, \gamma_h)_{I_j} + \langle \widehat{\gamma}_h, \gamma_h \rangle_{I_j} - (\gamma_h, (\gamma_h)_y)_{I_j} = 0, \quad (2.17)$$

$$-((\omega_h)_s, (u_h)_s)_{I_j} + (\rho_h u_h, (u_h)_s)_{I_j} = 0, \quad (2.18)$$

$$((\omega_h)_s, (u_h)_s)_{I_j} - \langle \widehat{u}_h, (u_h)_s \rangle_{I_j} + ((u_h)_s, (u_h)_{sy})_{I_j} = 0, \quad (2.19)$$

$$-(\gamma_h, (\rho_h)_s)_{I_j} + (\frac{1}{2} u_h^2, (\rho_h)_s)_{I_j} = 0. \quad (2.20)$$

Summing up all equalities (2.17)–(2.20), we obtain

$$\begin{aligned} & (\rho_h u_h, (u_h)_s)_{I_j} + (\frac{1}{2} u_h^2, (\rho_h)_s)_{I_j} + \\ & \langle \widehat{\gamma}_h, \gamma_h \rangle_{I_j} - (\gamma_h, (\gamma_h)_y)_{I_j} - \langle \widehat{u}_h, (u_h)_s \rangle_{I_j} + ((u_h)_s, (u_h)_{sy})_{I_j} = 0, \end{aligned}$$

which can be written as

$$\frac{1}{2} \frac{d}{ds} \int_{I_j} \rho_h u_h^2 dy + \Phi_{j+\frac{1}{2}} - \Phi_{j-\frac{1}{2}} + \Theta_{j-\frac{1}{2}} = 0, \quad (2.21)$$

where the numerical entropy fluxes are given by

$$\Phi = \widehat{\gamma}_h \gamma_h^- - \frac{1}{2} (\gamma_h^-)^2 - \langle \widehat{u}_h, (u_h)_s^- \rangle + \frac{1}{2} ((u_h)_s^-)^2$$

and the extra term Θ is

$$\Theta = (-\widehat{\gamma}_h + \{\{\gamma_h\}\}) \llbracket \gamma_h \rrbracket + (\langle \widehat{u}_h, (u_h)_s \rangle - \{\{u_h\}\}) \llbracket (u_h)_s \rrbracket.$$

Therefore the choices of $\widehat{\gamma}_h, \widehat{u}_h$ in (2.16) concern the conservativeness of the DG scheme. According to the parameters α, β, μ , we give two cases:

$$H_0 \text{ conserved DG scheme } \alpha = \beta = \mu = 0: \quad \Theta = 0; \quad (2.22)$$

$$H_0 \text{ dissipative DG scheme } \alpha = 0, \beta = \frac{1}{2}, \mu = \frac{1}{2}: \quad \Theta = \frac{1}{2} (\llbracket \gamma^2 \rrbracket + \llbracket u_s^2 \rrbracket) \geq 0. \quad (2.23)$$

Summing up the cell entropy equalities (2.21) and (2.22), (2.21) and (2.23), respectively, then we get

$$\frac{1}{2} \frac{d}{ds} \int_I \rho_h u_h^2 dy = 0, \quad H_0 \text{ conserved DG scheme,}$$

$$\frac{1}{2} \frac{d}{ds} \int_I \rho_h u_h^2 dy \leq 0, \quad H_0 \text{ dissipative DG scheme.} \quad \square$$

In the numerical test Example 4.2, it shows that the dissipative scheme with parameters (2.23) can achieve the optimal convergence rate for both u and ρ no matter k is odd or even. However, the order of accuracy for the H_0 conserved DG scheme (2.22) is k -th for odd k , $(k+1)$ -th for even k on uniform meshes. With nonuniform meshes, the H_0 conserved DG scheme is suboptimal order of accuracy regardless of the parity of the polynomial degrees. The choices of these parameters are not unique, but the above numerical fluxes in the dissipative scheme can minimize the stencil as in [46].

2.2.3. H_1 conserved DG scheme

In this section, we construct another discontinuous Galerkin scheme which preserves the quantity H_1 of the CD system (2.2) which links the Hamiltonian E_1 of the short pulse equation through the hodograph transformation. First, we rewrite the CD system as a first order system

$$\begin{cases} \rho_s + u\omega = 0, \\ w_s = \rho u, \\ \omega = u_y. \end{cases} \quad (2.24)$$

Then the semi-discrete LDG numerical scheme can be constructed as: Find $u_h, \omega_h, \rho_h \in V_h^k$ such that

$$\begin{cases} ((\rho_h)_s, \phi)_{I_j} + (u_h \omega_h, \phi)_{I_j} = 0, & (a) \\ ((\omega_h)_s, \varphi)_{I_j} = (\rho_h u_h, \varphi)_{I_j}, & (b) \\ (\omega_h, \psi)_{I_j} = \langle \hat{u}_h, \psi_y \rangle_{I_j} - (u_h, \psi_y)_{I_j}, & (c) \end{cases} \quad (2.25)$$

for all test functions $\phi, \varphi, \psi \in V_h^k$ and $I_j \in \mathcal{T}_h$. The numerical flux is taken as $\hat{u}_h = u_h^+$. Numerically, the optimal $(k+1)$ -th order of accuracy can be obtained for both u_h, ρ_h .

Proposition 2.3. (H_1 conservation) *The semi-discrete DG numerical scheme (2.25) can preserve the quantity $H_1(\rho_h, \omega_h) = \int_I (\rho_h^2 + \omega_h^2) dy$ spatially.*

Proof. By taking the test functions $\phi = \rho_h, \varphi = \omega_h$ in (2.25), we obtain

$$\begin{aligned} ((\rho_h)_s, \rho_h)_{I_j} + (u_h \omega_h, \rho_h)_{I_j} &= 0, \\ ((\omega_h)_s, \omega_h)_{I_j} &= (\rho_h u_h, \omega_h)_{I_j}. \end{aligned}$$

Summing up over all $I_j \in \mathcal{T}_h$, it implies that

$$\frac{1}{2} \frac{d}{ds} \int_I \rho_h^2 + \omega_h^2 dy = 0. \quad \square$$

In what follows, we prepare to give the a priori error estimate for the H_1 conserved DG scheme. The standard L^2 projection of a function ζ with $k+1$ continuous derivatives into space V_h^k , is denoted by \mathcal{P} , i.e., for each I_j

$$(\mathcal{P}\zeta - \zeta, \phi)_{I_j} = 0, \quad \forall \phi \in P^k(I_j),$$

and the special projections \mathcal{P}^\pm into V_h^k satisfy, for each I_j

$$(\mathcal{P}^+\zeta - \zeta, \phi)_{I_j} = 0, \quad \forall \phi \in P^{k-1}(I_j), \quad \text{and} \quad \mathcal{P}^+\zeta(y_{j-\frac{1}{2}}^+) = \zeta(y_{j-\frac{1}{2}}),$$

$$(\mathcal{P}^-\zeta - \zeta, \phi)_{I_j} = 0, \quad \forall \phi \in P^{k-1}(I_j), \quad \text{and} \quad \mathcal{P}^-\zeta(y_{j+\frac{1}{2}}^-) = \zeta(y_{j+\frac{1}{2}}).$$

For the projections mentioned above, it is easy to show [6] that

$$\|\zeta^e\|_{L^2(I)} + h^{\frac{1}{2}} \|\zeta^e\|_{L^\infty(I)} + h^{\frac{1}{2}} \|\zeta^e\|_{L^2(\partial I)} \leq Ch^{k+1}, \quad (2.26)$$

where $\zeta^e = \zeta - \mathcal{P}\zeta$ or $\zeta^e = \zeta - \mathcal{P}^\pm\zeta$, and the positive constant C only depends on ζ . There is an inverse inequality we will use in the subsequent proof. For $\forall u_h \in V_h^k$, there exists a positive constant σ (we call it the inverse constant), such that

$$\|u_h\|_{L^2(\partial I)} \leq \sigma h^{-\frac{1}{2}} \|u_h\|_{L^2(I)}, \quad (2.27)$$

where $\|u_h\|_{L^2(\partial I)} = \sqrt{\sum_{j=1}^{N+1} ((u_h)_{j+\frac{1}{2}}^-)^2 + ((u_h)_{j-\frac{1}{2}}^+)^2}$.

First, we write the error equations of the H_1 conserved DG scheme as follows:

$$((\rho - \rho_h)_s, \varphi)_{I_j} = -(u\omega - u_h\omega_h, \varphi)_{I_j}, \quad (2.28)$$

$$((\omega - \omega_h)_s, \phi)_{I_j} = (\rho u - \rho_h u_h, \phi)_{I_j}, \quad (2.29)$$

$$(\omega - \omega_h, \psi)_{I_j} = \langle \widehat{u - u_h}, \psi \rangle_{I_j} - (u - u_h, \psi_y)_{I_j}, \quad (2.30)$$

and denote

$$\begin{aligned} \eta^u &= u - \mathcal{P}^+ u, \quad \xi^u = \mathcal{P}^+ u - u_h, \\ \eta^\rho &= \rho - \mathcal{P} \rho, \quad \xi^\rho = \mathcal{P} \rho - \rho_h, \\ \eta^\omega &= \omega - \mathcal{P} \omega, \quad \xi^\omega = \mathcal{P} \omega - \omega_h. \end{aligned} \quad (2.31)$$

To deal with the term ξ^u , we need to establish a relationship between ξ^u and ξ^ω in following lemma.

Lemma 2.4. *The $\xi^u, \xi^\omega, \eta^\omega$ are defined in (2.31), then there exists a positive constant $C_{\sigma,p}$ independent of h but depending on inverse constant σ and Poincaré constant C_p , such that*

$$\|\xi^u\|_{L^2(I)} \leq C_{\sigma,p} (\|\xi^\omega\|_{L^2(I)} + \|\eta^\omega\|_{L^2(I)}).$$

Proof. By Poincaré Friedrichs inequality in Chapter 10 of [5], we have

$$\|\xi^u\|_{L^2(I)} \leq C_p \left[\|\xi_y^u\|_{L^2(I)} + h^{-\frac{1}{2}} \|\llbracket \xi^u \rrbracket\|_{L^2(\partial I)} \right]$$

where

$$\|\xi_y^u\|_{L^2(I)} = \left(\sum_{I_j \in \mathcal{T}_h} \int_{I_j} (\xi_y^u)^2 dy \right)^{\frac{1}{2}}, \quad \|\llbracket \xi^u \rrbracket\|_{L^2(\partial I)} = \left(\sum_{j=1}^{N+1} \llbracket \xi^u \rrbracket_{j-\frac{1}{2}}^2 \right)^{\frac{1}{2}}.$$

The inequality (4.17) in [33] gives

$$\left[\|\xi_y^u\|_{L^2(I)} + h^{-\frac{1}{2}} \|\llbracket \xi^u \rrbracket\|_{L^2(\partial I)} \right] \leq C_\sigma (\|\xi^\omega\|_{L^2(I)} + \|\eta^\omega\|_{L^2(I)}),$$

which implies that

$$\|\xi^u\|_{L^2(I)} \leq C_{\sigma,p} (\|\xi^\omega\|_{L^2(I)} + \|\eta^\omega\|_{L^2(I)}). \quad \square$$

Theorem 2.5. *It is assumed that the system (2.24) with the Dirichlet boundary condition has a smooth solution u, ρ, ω . Let u_h, ρ_h, ω_h be the numerical solution of the semi-discrete DG scheme (2.25). And there exists that initial conditions $u_h^0, \rho_h^0, \omega_h^0$ satisfy the following approximation property*

$$\|u^0 - u_h^0\|_{L^2(I)} + \|\rho^0 - \rho_h^0\|_{L^2(I)} + \|\omega^0 - \omega_h^0\|_{L^2(I)} \leq Ch^{k+1}.$$

Thereafter for regular partitions of $I = (y_L, y_R)$, and the finite element space V_h^k with $k \geq 0$, there holds the following error estimate

$$\|u - u_h\|_{L^2(I)} + \|\omega - \omega_h\|_{L^2(I)} + \|\rho - \rho_h\|_{L^2(I)} \leq Ch^{k+1},$$

where the positive constant C depends on the final time T and the exact solutions.

Proof. We rewrite the error equation (2.28), (2.29) as

$$\begin{aligned} ((\xi^\rho + \eta^\rho)_s, \varphi)_{I_j} &= (-u\omega + u_h\omega_h, \varphi)_{I_j} \\ &= (-\omega(\xi^u + \eta^u) - u_h(\xi^\omega + \eta^\omega), \varphi)_{I_j}, \\ ((\xi^\omega + \eta^\omega)_s, \phi)_{I_j} &= (\rho u - \rho_h u_h, \phi)_{I_j} \\ &= (\rho(\xi^u + \eta^u)_{I_j} + u_h(\xi^\rho + \eta^\rho), \phi)_{I_j}. \end{aligned}$$

Taking the test functions $\varphi = \xi^\rho$, $\phi = \xi^\omega$, we have

$$\begin{aligned}(\xi_s^\rho, \xi^\rho)_{I_j} &= (-\eta_s^\rho, \xi^\rho)_{I_j} - (\omega(\xi^u + \eta^u) + u_h(\xi^\omega + \eta^\omega), \xi^\rho)_{I_j}, \\(\xi_s^\omega, \xi^\omega)_{I_j} &= (-\eta_s^\omega, \xi^\omega)_{I_j} + (\rho(\xi^u + \eta^u) + u_h(\xi^\rho + \eta^\rho), \xi^\omega)_{I_j}.\end{aligned}$$

Summing up over all interval I_j and omitting the subscript I , we obtain

$$\begin{aligned}(\xi_s^\rho, \xi^\rho) + (\xi_s^\omega, \xi^\omega) &= (-\eta_s^\rho - \omega(\xi^u + \eta^u) - u_h\eta^\omega, \xi^\rho) + (-\eta_s^\omega + \rho(\xi^u + \eta^u) + \eta^\rho u_h, \xi^\omega) \\&= (-\eta_s^\rho - \mathcal{P}\omega(\xi^u + \eta^u) - u\eta^\omega, \xi^\rho) + (-\eta_s^\omega + \mathcal{P}\rho(\xi^u + \eta^u) + u\eta^\rho, \xi^\omega) \\&= (A, \xi^\rho) + (B, \xi^\omega) - (\mathcal{P}\omega\xi^u, \xi^\rho) + (\mathcal{P}\rho\xi^u, \xi^\omega).\end{aligned}$$

By the Cauchy-Schwarz and arithmetic-geometric mean inequalities, the equation becomes

$$\frac{d}{dt}(\|\xi^\omega\|_{L^2(I)}^2 + \|\xi^\rho\|_{L^2(I)}^2) \leq K + \frac{1}{2}(1 + C_{\omega,\rho})(\|\xi^\omega\|_{L^2(I)}^2 + \|\xi^\rho\|_{L^2(I)}^2) + C_{\omega,\rho} \|\xi^u\|_{L^2(I)}^2 \quad (2.32)$$

where

$$\begin{aligned}A &= -\eta_s^\rho - \mathcal{P}\omega\eta^u - u\eta^\omega, \quad B = -\eta_s^\omega + \mathcal{P}\rho\eta^u + u\eta^\rho, \\K &= \frac{1}{2}(\|A\|_{L^2(I)}^2 + \|B\|_{L^2(I)}^2), \quad C_{\omega,\rho} = \max(c_\rho, c_\omega).\end{aligned}$$

Here, we need to interpret the constants we mentioned above. We denote by C_* all positive constants independent of h , which depends on the subscript $*$.

Using Lemma 2.4 in the above inequality (2.32), we get

$$\frac{d}{dt}(\|\xi^\omega\|_{L^2(I)}^2 + \|\xi^\rho\|_{L^2(I)}^2) \leq \tilde{K} + C_{\sigma,\omega,\rho}(\|\xi^\omega\|_{L^2(I)}^2 + \|\xi^\rho\|_{L^2(I)}^2),$$

where

$$\tilde{K} = \frac{1}{2}(\|A\|_{L^2(I)}^2 + \|B\|_{L^2(I)}^2) + C_{\sigma,\omega,\rho} \|\eta^\omega\|_{L^2(I)}^2, \quad C_{\sigma,\omega,\rho} = \frac{1}{2}(1 + C_{\omega,\rho} + C_{\sigma,\omega,\rho}).$$

By the Gronwall's inequality, we have

$$\|\xi^\omega\|_{L^2(I)}^2 + \|\xi^\rho\|_{L^2(I)}^2 \leq Ch^{2k+2}.$$

Lemma 2.4 also implies that

$$\|\xi^u\|_{L^2(I)}^2 \leq Ch^{2k+2}.$$

Then Theorem 2.5 follows by the triangle inequality and the interpolating property. \square

2.2.4. Integration DG scheme

Instead of the scheme (2.25c) to solve u_h from ω_h , we can also integrate the equation $u_y = \omega$ directly referring to [41]. We give an integration DG scheme defined as follows: Find $u_h \in V_h^{k+1}$, $\rho_h, \omega_h \in V_h^k$, such that, for all test functions $\phi, \varphi \in V_h^k$ and $I_j \in \mathcal{T}_h$

$$\begin{cases} ((\rho_h)_s, \phi)_{I_j} + (u_h \omega_h, \phi)_{I_j} = 0, \\ ((\omega_h)_s, \varphi)_{I_j} = (\rho_h u_h, \varphi)_{I_j}, \\ u_h(y, s)|_{I_j} = u_h(y_{j+\frac{1}{2}}, s) - \int_y^{y_{j+\frac{1}{2}}} \omega_h(\xi, s) d\xi, \end{cases} \quad (2.33)$$

with the Dirichlet boundary condition $u_h(y_{N+\frac{1}{2}}, s) = u(y_R, s)$. Here, u_h is no longer in V_h^k space but in V_h^{k+1} space and continuous. Numerically, this scheme can obtain the optimal order of accuracy, i.e. $(k+2)$ -th order for u_h , and $(k+1)$ -th order for ρ_h .

Remark 2.1. It is notable that our integration DG scheme (2.33) is based on the H_1 conserved DG scheme (2.25). Actually, following the H_0 conserved DG scheme (2.14), we have another integration DG scheme: Find $u_h \in V_h^{k+1}$, $\rho_h, \omega_h, \gamma_h \in V_h^k$ such that

$$\begin{cases} ((\rho_h)_s, \phi)_{I_j} + \langle \widehat{\gamma}_h, \phi \rangle_{I_j} - (\gamma_h, \phi_y)_{I_j} = 0, & (a) \\ ((\omega_h)_s, \varphi)_{I_j} = (\rho_h u_h, \varphi)_{I_j}, & (b) \\ (\gamma_h, \eta)_{I_j} = (\frac{1}{2} u_h^2, \eta)_{I_j}, & (c) \\ u_h(y, s)|_{I_j} = u_h(y_{j+\frac{1}{2}}, s) - \int_y^{y_{j+\frac{1}{2}}} \omega_h(\xi, s) d\xi, & (d) \end{cases} \quad (2.34)$$

for all test functions $\phi, \varphi, \eta \in V_h^k$ and $I_j \in \mathcal{T}_h$. The only difference between those two integration DG schemes is the L^2 projection (2.34c). Numerically, there is little difference on accuracy and conserved quantities H_0, H_1 . In the following sections, the integration DG scheme we mention refers to the numerical scheme (2.33).

To prove the error estimate of this integration scheme, we introduce the following lemma to build the relationship between ξ^u and ξ^ω .

Lemma 2.6. *In this lemma, u, ω is the exact solution of CD system (2.24) with the Dirichlet boundary, ω is the derivative of u with respect to y . The numerical solutions u_h, ω_h of the integration DG scheme (2.33) for CD system satisfy $(u_h)_y = \omega_h$, and $\xi^u, \xi^\omega, \eta^u, \eta^\omega$ are defined in (2.31), then we have the following relationship:*

$$\|\xi_y^u\|_{L^2(I)} + h^{-\frac{1}{2}} \|\llbracket \xi^u \rrbracket\|_{L^2(I)} \leq C_\sigma (\|\xi^\omega\|_{L^2(I)} + \|\eta^\omega\|_{L^2(I)} + h^{-1} \|\eta^u\|_{L^2(I)}) \quad (2.35)$$

where the positive constant C_σ depends on the inverse constant σ .

Proof. First we write the error equation

$$\xi_y^u + \eta_y^u = \xi^\omega + \eta^\omega. \quad (2.36)$$

Here we take a test function ϕ as follows:

$$\phi(y)_{I_j} = \xi_y^u(y) - (\xi_y^u)_{j+\frac{1}{2}}^- L_{k+1}(\zeta)$$

where L_k is the standard Legendre polynomial of degree $k-1$ in $[-1, 1]$, $\zeta = 2(y - y_j)/h_j$. We have $L_k(1) = 1$ and L_k is orthogonal to any polynomials with degree at most $k-1$. Therefore we obtain some relevant properties $\phi_{j+\frac{1}{2}}^- = 0$, $(\xi_y^u, \phi)_{I_j} = (\xi_y^u, \xi_y^u)_{I_j}$. Then we multiply the error equation (2.36) by test function $\phi(y)$ and integrate it over I_j , which follows that

$$\begin{aligned} (\xi_y^u, \phi)_{I_j} + (\eta_y^u, \phi)_{I_j} &= (\xi^\omega, \phi)_{I_j} + (\eta^\omega, \phi)_{I_j}, \\ (\xi_y^u, \xi_y^u)_{I_j} + (\eta_y^u)_{j+\frac{1}{2}}^- \phi_{j+\frac{1}{2}}^- - (\eta^u)_{j-\frac{1}{2}}^+ \phi_{j-\frac{1}{2}}^+ - (\eta^u, \phi_y)_{I_j} &= (\xi^\omega, \phi)_{I_j} + (\eta^\omega, \phi)_{I_j}, \\ (\xi_y^u, \xi_y^u)_{I_j} &= (\xi^\omega, \phi)_{I_j} + (\eta^\omega, \phi)_{I_j}. \end{aligned}$$

Since $\|L_k(\zeta)\|_{L^2(I_j)} \leq Ch_j^{\frac{1}{2}}$, we use Cauchy-Schwarz inequality and the inverse property (2.27), and obtain

$$\begin{aligned} \|\xi_y^u\|_{L^2(I_j)}^2 &\leq (\|\xi_y^u\|_{L^2(I_j)} + |(\xi_y^u)_{j+\frac{1}{2}}^-| \|L_k(\zeta)\|_{L^2(I_j)}) (\|\xi^\omega\|_{L^2(I_j)}^2 + \|\eta^\omega\|_{L^2(I_j)}^2) \\ &\leq C_\sigma \|\xi_y^u\|_{L^2(I_j)} (\|\xi^\omega\|_{L^2(I_j)}^2 + \|\eta^\omega\|_{L^2(I_j)}^2). \end{aligned} \quad (2.37)$$

Hence we arrive at

$$\|\xi_y^u\|_{L^2(I_j)} \leq C_\sigma (\|\xi^\omega\|_{L^2(I_j)}^2 + \|\eta^\omega\|_{L^2(I_j)}^2).$$

Next, for the boundary term $\llbracket \xi^u \rrbracket_{j-\frac{1}{2}}$, the deduction process is as follows:

$$\llbracket \xi^u \rrbracket_{j-\frac{1}{2}} = [\mathcal{P}^+ u - u_h]_{j-\frac{1}{2}} = [\mathcal{P}^+ u]_{j-\frac{1}{2}} = [\mathcal{P}^+ u - u]_{j-\frac{1}{2}} = \llbracket \eta^u \rrbracket_{j-\frac{1}{2}}.$$

Here the equalities hold due to the continuity of u and u_h . Taking account of the projection error (2.26), we have

$$\|\llbracket \xi^u \rrbracket\|_{L^2(I_j)} = \|\llbracket \eta^u \rrbracket\|_{L^2(I_j)} \leq Ch^{-\frac{1}{2}} \|\eta^u\|_{L^2(I_j)}$$

Finally, by summing over all cells I_j it follows the result (2.35) \square

Next, we imitate Theorem 2.5 and give the error estimate for the integration DG scheme (2.33).

Theorem 2.7. It is assumed that the system (2.24) with the Dirichlet boundary condition has a smooth solution u, ρ, ω . Let u_h, ρ_h, ω_h be the numerical solution of the semi-discrete DG scheme (2.33). And there exists that initial conditions $u_h^0, \omega_h^0, \rho_h^0$ satisfy the following approximation property

$$\|u^0 - u_h^0\|_{L^\infty(I)} + \|\rho^0 - \rho_h^0\|_{L^2(I)} + \|\omega^0 - \omega_h^0\|_{L^2(I)} \leq Ch^{k+1}.$$

Thereafter for a regular partitions of $I = (y_L, y_R)$, and the finite element spaces V_h^k and V_h^{k+1} with $k \geq 0$, there holds the following error estimates

$$\|u - u_h\|_{L^\infty(I)} + \|\omega - \omega_h\|_{L^2(I)} + \|\rho - \rho_h\|_{L^2(I)} \leq Ch^{k+1}$$

where the positive constant C depends on the final time T and the exact solutions.

Proof. First, we write the error equations of the integration DG scheme (2.33) as follows:

$$\begin{cases} ((\rho - \rho_h)_s, \varphi)_{I_j} = -(u\omega - u_h\omega_h, \varphi)_{I_j}, & (a) \\ ((\omega - \omega_h)_s, \phi)_{I_j} = (\rho u - \rho_h u_h, \phi)_{I_j}, & (b) \\ (u - u_h)(y) = (u - u_h)(y_{j+\frac{1}{2}}) - \int_{y_j}^{y_{j+\frac{1}{2}}} (\omega - \omega_h)(\zeta) d\zeta. & (c) \end{cases} \quad (2.38)$$

Then the process of this proof is similar to the proof of Theorem 2.5. We can adopt the proof of Theorem 2.5 until estimate (2.32). The relationship between ξ^u and ξ^w for the integration DG scheme which has been provided in Lemma 2.6 guarantees that the proof can be continued. Under this circumstance, $u \in V_h^{k+1}$ and $\|\eta^u\| < Ch^{k+2}$. So we still have the same result as Theorem 2.5,

$$\|\xi^\omega\|_{L^2(I)}^2 + \|\xi^\rho\|_{L^2(I)}^2 \leq Ch^{2k+2}.$$

Then followed by the triangle inequality and the interpolating property, there holds

$$\|\omega - \omega_h\|_{L^2(I)} + \|\rho - \rho_h\|_{L^2(I)} \leq Ch^{k+1}.$$

Here, we can obtain the L^∞ error estimate for u_h . For $\forall y \in [y_L, y_R]$, we apply Cauchy-Schwarz inequality on error equation (2.38c), and the following estimate holds

$$|(u - u_h)(y)| = \left| (u - u_h)(y_R) + \int_y^{y_R} (\omega - \omega_h)(\xi) d\xi \right| \leq C \|\omega - \omega_h\|_{L^2(I)}. \quad (2.39)$$

The boundary term vanishes in (2.39) due to the boundary condition $u(y_R, s) = u_h(y_{N+\frac{1}{2}}, s)$. Thus we arrive at $\|u - u_h\|_{L^\infty} \leq Ch^{k+1}$. \square

2.3. The sine-Gordon equation

There exists some short pulse type equations which are failed to be transformed into the corresponding CD systems to solve, e.g., some examples in Section 3. In this section, we can adopt an alternative approach by linking the short pulse equation (2.1) with the sine-Gordon equation.

First, we consider the sine-Gordon equation

$$z_{ys} = \sin z, \quad z \in \mathbb{R}, \quad (2.40)$$

where s denotes the temporal coordinate, y is the spatial scale and $y \in I = [y_L, y_R]$. The hodograph transformation between the short pulse equation and the sine-Gordon equation is as follows:

$$\begin{cases} \frac{\partial}{\partial y} = \cos z \frac{\partial}{\partial x}, \\ \frac{\partial}{\partial s} = \frac{\partial}{\partial t} - \frac{(z_s)^2}{2} \frac{\partial}{\partial x}. \end{cases}$$

The parametric representation of the solution of the short pulse equation (2.1) is

$$u = z_s(y, s), \quad x = x(y_0, s) + \int_{y_0}^y \cos z \, dy.$$

The sine-Gordon equation has a conserved quantity $H_2 = \int_I z_s^2 \, dy$ which can be preserved discretely in the following DG scheme.

2.3.1. DG scheme for sine-Gordon equation

In this subsection, we develop the DG scheme for the sine-Gordon equation (2.40). We divide the sine-Gordon equation into these first-order equations

$$\begin{cases} \omega_s = \eta, \\ \eta = \sin z, \\ \omega = z_y. \end{cases}$$

The semi-discrete DG numerical method for sine-Gordon equation is defined as follows: Find $z_h, \eta_h, \omega_h \in V_h^k$, such that, for all test functions $\varphi, \phi, \psi \in V_h^k$ and $I_j \in \mathcal{T}_h$

$$\begin{cases} ((\omega_h)_s, \varphi)_{I_j} = (\eta_h, \varphi)_{I_j}, \\ (\eta_h, \phi)_{I_j} = (\sin z_h, \phi)_{I_j}, \\ (\omega_h, \psi)_{I_j} = \langle \widehat{z}_h, \psi \rangle_{I_j} - (z_h, \psi_y)_{I_j}, \end{cases} \quad (2.41)$$

where the numerical flux is $\widehat{z}_h = z_h^+$. Numerically, this scheme can achieve the optimal order of accuracy for z_h .

To maintain the quantity H_2 conserved, we can also choose a special numerical flux \widehat{z}_h

$$\widehat{z}_h = \begin{cases} \frac{[z_h \eta_h] - [\cos z_h]}{[\eta_h]}, & [\eta_h] \neq 0, \\ z_h, & [\eta_h] = 0, \end{cases}$$

which makes this scheme H_2 conservative. But in the actual computation, this conservative scheme will increase the complexity for solving a nonlinear system. For the convenience of the simulation, we adopt the numerical flux $\widehat{z}_h = z_h^+$ for the DG scheme (2.41) in our numerical tests. Here, the Dirichlet boundary condition is adopted for variable z . For the case of periodic boundary condition, the detailed discussion is provided in [32].

2.3.2. Integration DG scheme for sine-Gordon equation

We can also solve $\omega = z_y$ by integration directly as the scheme (2.33) in Section 2.2.4. The semi-discrete integration DG numerical scheme for sine-Gordon equation (2.40) is formulated as: Find $z_h \in V_h^{k+1}$, $\eta_h, \omega_h \in V_h^k$, such that, for all test functions $\varphi, \phi \in V_h^k$ and $I_j \in \mathcal{T}_h$,

$$\begin{cases} ((\omega_h)_s, \varphi)_{I_j} = (\eta_h, \varphi)_{I_j}, & (a) \\ (\eta_h, \phi)_{I_j} = (\sin z_h, \phi)_{I_j}, & (b) \\ z_h(y, s)|_{I_j} = z_h(y_{j+\frac{1}{2}}, s) - \int_y^{y_{j+\frac{1}{2}}} \omega_h(\xi, s) d\xi, & (c) \end{cases} \quad (2.42)$$

with the Dirichlet boundary condition $z_h(y_{N+\frac{1}{2}}, s) = z(y_R, s)$. Similarly, this scheme can achieve the optimal $(k+2)$ -th order of accuracy for z_h numerically.

Since $u = z_s$, when we obtain z_h in each time level, u_h^n can be computed by a fourth order approximation

$$u_h^n = \frac{2z_h^{n+1} + 3z_h^n - 6z_h^{n-1} + z_h^{n-2}}{6\Delta s}.$$

Here, we just give one of approximation methods to get u_h by z_h as an example, and this discretization method is not unique.

3. Extensions to other cases

In this section, we consider some generalized short pulse type equations. Similar numerical schemes including H_0 , H_1 conserved DG schemes and integration DG scheme in Section 2.2 for the corresponding CD systems, DG scheme and integration DG scheme in Section 2.3 for sine-Gordon type equations can be also adopted to solve these generalized short pulse type equations via hodograph transformations. For simplicity, we just introduce these generalized equations and the conservative quantities considered in the numerical schemes.

3.1. The coupled short pulse equation

The short pulse equation can be generalized to the coupled short pulse equations

$$\begin{cases} u_{xt} = u + \frac{1}{2}(uvu_x)_x, \\ v_{xt} = v + \frac{1}{2}(uvv_x)_x, \end{cases} \quad u, v \in \mathbb{R}, \quad (3.1)$$

Table 3.1The conserved quantities H_0 , H_1 for three generalized CD systems.

	Coupled CD (3.2)	Complex CD (3.4)	Coupled CD in complex form (3.6)
H_0	$\int \rho u v dy$	$\int \rho u ^2 dy$	$\int \rho (u ^2 + v ^2) dy$
H_1	$\int \rho^2 + u_y v_y dy$	$\int \rho^2 + u_y ^2 dy$	$\int \rho^2 + u_y ^2 + v_y ^2 dy$

which can be converted into a coupled CD system

$$\rho_s + \frac{1}{2}(uv)_y = 0, \quad u_{ys} = \rho u, \quad v_{ys} = \rho v, \quad (3.2)$$

proposed by Konno and Kakuhata in [19]. For the coupled short pulse equation (3.1), we set $u, v \in \mathbb{C}$ and $v = u^*$ which denotes the complex conjugate of u . Then we have complex short pulse equation derived from [14]

$$u_{xt} = u + \frac{1}{2}(|u|^2 u_x)_x, \quad u \in \mathbb{C}, \quad (3.3)$$

which is related to the complex CD system

$$\rho_s + \frac{1}{2}|u|_y^2 = 0, \quad u_{ys} = \rho u, \quad u_{ys}^* = \rho u^*. \quad (3.4)$$

According to the real-valued case, we also give the complex form of the coupled short pulse equation,

$$\left. \begin{aligned} u_{xt} &= u + \frac{1}{2}(|u|^2 + |v|^2)u_x, \\ v_{xt} &= v + \frac{1}{2}(|v|^2 + |u|^2)v_x, \end{aligned} \right\} u, v \in \mathbb{C}. \quad (3.5)$$

Through the corresponding hodograph transformation, it can be transformed into

$$\rho_s + \frac{1}{2}(|u|^2)_y + \frac{1}{2}(|v|^2)_y = 0, \quad u_{sy} = \rho u, \quad v_{sy} = \rho v. \quad (3.6)$$

Similar to the short pulse equation (2.1), the corresponding H_0 , H_1 conserved DG schemes and integration DG scheme can be constructed to solve above three short pulse type equations (3.1), (3.3), (3.5), respectively. Here, we list the conserved quantities H_0 , H_1 in Table 3.1.

3.2. The modified short pulse equation

For nonlinear wave equation

$$u_{xt} = u + au^2 u_{xx} + buu_x^2,$$

if its coefficient ratio a/b equals 1 instead of $\frac{1}{2}$, then we obtain the modified short pulse equation after rescaling the variable u ,

$$u_{xt} = u + \frac{1}{2}u(u^2)_{xx}, \quad u \in \mathbb{R}. \quad (3.7)$$

It can be converted to a modified CD system [25]

$$\rho_s + (u^2)_y = 0, \quad u_{ys} = (2\rho - 1)u, \quad (3.8)$$

for which we can build H_0 , H_1 conserved and integration DG schemes.

Next, some generalized modified short pulse equation will be introduced. It is worth to mention that there is one type generalized modified short pulse equation in Section 3.2.2, which can not be transformed into the CD system but only the sine-Gordon equations through the hodograph transformation.

3.2.1. The generalized modified short pulse systems

The modified short pulse equation

$$\left. \begin{aligned} u_{xt} &= u + \frac{1}{2}v(u^2)_{xx}, \\ v_{xt} &= v + \frac{1}{2}u(v^2)_{xx}, \end{aligned} \right\} u, v \in \mathbb{R}, \quad (3.9)$$

connects with the coupled modified CD system

$$\rho_s + (uv)_y = 0, \quad u_{ys} = (2\rho - 1)u, \quad v_{ys} = (2\rho - 1)v. \quad (3.10)$$

Table 3.2The conserved quantities H_0 , H_1 for three generalized MCD systems.

	MCD (3.8)	Complex MCD (3.10)	Defocusing complex MCD (3.12)
H_0	$\int (2\rho - 1)u^2 dy$	$\int (2\rho - 1)uv dy$	$\int (2\rho - 1) u ^2 dy$
H_1	$\int \rho^2 + u_y^2 dy$	$\int \rho^2 + u_y v_y dy$	$\int \rho^2 + u_y ^2 dy$

When $u, v \in \mathbb{C}$ and $v = u^*$ in (3.9), the focusing and defocusing type of complex modified short pulse equation mentioned in [31,15,16] are

$$u_{xt} = u \pm \frac{1}{2}u^*(u^2)_{xx}, \quad u \in \mathbb{C}, \quad (3.11)$$

and the corresponding CD system is

$$\rho_s \pm |u|_y^2 = 0, \quad u_{ys} = (2\rho - 1)u, \quad u_{ys}^* = (2\rho - 1)u^*. \quad (3.12)$$

Similarly, we can develop the corresponding H_0 , H_1 conserved DG schemes and integration DG scheme to solve the modified short pulse type equations (3.7), (3.9), (3.11) via the hodograph transformations. The conserved quantities H_0 , H_1 are contained in Table 3.2.

3.2.2. Sine-Gordon type equations

The modified short pulse equation (3.7) is linked with the sine-Gordon equation

$$z_{ys} = \sin z \cos z$$

which is equivalent to $z_{ys} = \frac{1}{2} \sin 2z$. Similarly, we can develop DG schemes for the sine-Gordon equation to solve the modified short pulse equation as in Section 2.3.

We consider another integrable generalization of the modified short pulse equation, so called the novel coupled short pulse equation proposed by Feng in [11]

$$\left. \begin{aligned} u_{xt} &= u + \frac{1}{6}(u^3)_{xx} + \frac{1}{2}v^2 u_{xx}, \\ v_{xt} &= v + \frac{1}{6}(v^3)_{xx} + \frac{1}{2}u^2 v_{xx}, \end{aligned} \right\} \quad u, v \in \mathbb{R}, \quad (3.13)$$

which is failed to be transformed to the CD system. But it can be transformed to the following two-component sine-Gordon system

$$z_{ys} = \sin z, \quad \tilde{z}_{ys} = \sin \tilde{z}, \quad (3.14)$$

by the hodograph transformation

$$\left\{ \begin{aligned} \frac{\partial}{\partial y} &= \frac{1}{2}(\cos z + \cos \tilde{z}) \frac{\partial}{\partial x}, \\ \frac{\partial}{\partial s} &= \frac{\partial}{\partial t} - \frac{u^2 + v^2}{2} \frac{\partial}{\partial x}. \end{aligned} \right. \quad (3.15)$$

Therefore, we develop the DG and integration DG schemes for this coupled system (3.14) as we did for the sine-Gordon equation in Section 2.3.

4. Numerical experiments

In this section we will provide several numerical experiments to illustrate the accuracy and capability of the DG methods. Time discretization is the fourth order explicit Runge-Kutta method in [17]. This time discretization method may not ensure the conservativeness of fully discretization schemes. However, we will not address the issue of time discretization conservativeness in this paper. In the numerical experiments based on hodograph transformations subsequently, the Dirichlet boundary condition is imposed, while for the periodic boundary condition, we recommend the readers referring to [32,47]s. In order not to repeat, we always choose one of H_0 , H_1 conserved and integration DG schemes to profile the numerical solution in the subsequent numerical experiments.

4.1. Solve the short pulse equation directly

Example 4.1. In this example, smooth solutions with periodic boundary condition for the short pulse equation (2.1) are used to test the E_0 conserved DG method in Section 2.2.1. We list one of the exact solutions derived in [23], which is given by the exact solution of the sine-Gordon equation (2.40) in the coordinate (y, s) and need to be transformed to the coordinate (x, t) in the following test,

Table 4.3

Example 4.1, the solution (4.1) of the short pulse equation (2.1): E_0 conserved DG scheme with uniform meshes in computational domain $[0, T_p]$, at time $T = 1$. The parameters $\kappa = 0.65, a = 1.3, x_0 = \eta_0 = d = 0$.

N	p^1				p^2			
	$\ u - u_h\ _{L^2}$	Order	$\ u - u_h\ _{L^\infty}$	Order	$\ u - u_h\ _{L^2}$	Order	$\ u - u_h\ _{L^\infty}$	Order
40	2.05E-02	–	9.17E-02	–	2.10E-05	–	1.12E-04	–
80	1.09E-02	0.91	5.18E-02	0.82	2.30E-06	3.19	1.22E-05	3.19
160	5.49E-03	0.99	2.90E-02	0.84	2.41E-07	3.26	1.40E-06	3.13
320	2.76E-03	0.99	1.54E-02	0.91	3.19E-08	2.92	1.90E-07	2.88

Table 4.4

Example 4.1, the solution (4.1) of the short pulse equation (2.1): E_0 conserved DG scheme with nonuniform meshes ($2dx, dx, 2dx, dx, \dots$) in computational domain $[0, T_p]$, at time $T = 1$. The parameters $\kappa = 0.65, a = 1.3, x_0 = \eta_0 = d = 0$.

N	p^1				p^2			
	$\ u - u_h\ _{L^2}$	Order	$\ u - u_h\ _{L^\infty}$	Order	$\ u - u_h\ _{L^2}$	Order	$\ u - u_h\ _{L^\infty}$	Order
40	2.24E-02	–	9.57E-02	–	3.21E-04	–	1.51E-03	–
80	1.18E-02	0.93	5.44E-02	0.82	5.37E-05	2.58	2.69E-04	2.49
160	6.07E-03	0.95	3.05E-02	0.83	1.28E-05	2.07	9.35E-05	1.53
320	3.05E-03	0.99	1.67E-02	0.87	3.04E-06	2.08	2.08E-05	2.17

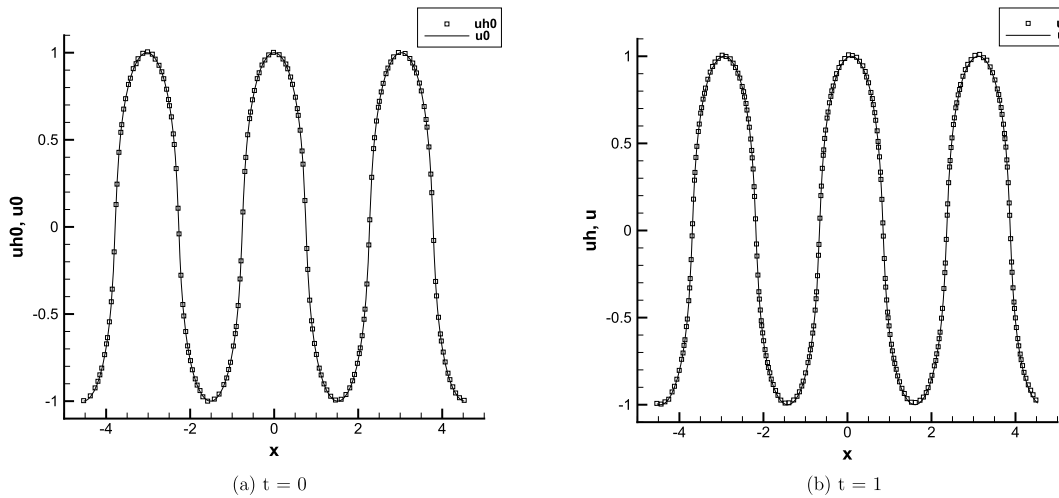


Fig. 4.1. Example 4.1, periodic solution (4.1) of the short pulse equation (2.1): E_0 conserved DG scheme with computational domain $[-1.5T_p, 1.5T_p]$ and $N = 160$ cells, p^2 elements at time $T = 0, 1$. The parameters $\kappa = 0.65, a = 1.3, x_0 = \eta_0 = d = 0$.

$$\begin{cases} u(y, s) = \frac{2\kappa}{a} cn(\eta, \kappa), \\ x(y, s) = x_0 + \frac{1}{a^2}(1 - 2\kappa^2)s + \frac{1}{a}(-\eta + 2E(\eta, \kappa)) + d, \\ \eta = ay - \frac{s}{a} + \eta_0, \end{cases} \quad (4.1)$$

where $cn(\eta, \kappa)$ is Jacobi's cn function. The period is computed by $T_p = \frac{4}{a}|-K(\kappa) + 2E(\kappa)|$, where $K(\kappa)$ and $E(\kappa)$ are the complete elliptic integrals of the first and second kinds, respectively [1].

The L^2 and L^∞ errors and the convergence rates with uniform and nonuniform meshes are contained in Table 4.3 and 4.4 respectively. On uniform meshes, for even k , we see the optimal order of accuracy, while for odd k , we can only have suboptimal order of accuracy. However, only suboptimal order of accuracy can be achieved on nonuniform meshes regardless of the parity of the polynomial degrees. Fig. 4.1 illustrates a typical periodic solution at $T = 1$ with the parameters $\kappa = 0.65, a = 1.3, x_0 = \eta_0 = d = 0$. This solution represents a periodic wavetrain traveling to the right with a constant velocity $V = 0.0917$.

4.2. Solve the short pulse type equations by transforming it to the CD systems

Example 4.2. This example is devoted to solve some loop-soliton solutions of the short pulse equation (2.1) by linking with CD system. We list the general determinant form of solution of the short pulse equation:

Table 4.5

Example 4.2, 1-soliton solution of the CD system (2.2): uniform meshes in the computational domain $[-10, 10]$, P^2 elements, at time $T = 10$. The parameters $p_1 = 1.0, \alpha_1 = 4.0$.

	N	$\ u - u_h\ _{L^2}$	Order	$\ u - u_h\ _{L^\infty}$	Order	$\ \rho - \rho_h\ _{L^2}$	Order	$\ \rho - \rho_h\ _{L^\infty}$	Order
H_0 Dissipative DG scheme	40	1.17E-02	-	8.00E-02	-	1.84E-02	-	2.30E-01	-
	80	3.97E-04	4.88	2.37E-03	5.08	6.68E-04	4.78	1.07E-02	4.43
	160	4.92E-05	3.01	2.78E-04	3.09	7.75E-05	3.11	1.17E-03	3.19
	320	6.85E-06	2.85	3.85E-05	2.85	1.03E-05	2.91	1.50E-04	2.97
H_0 Conserved DG scheme	40	7.92E-03	-	3.79E-02	-	6.59E-04	-	7.83E-03	-
	80	8.46E-05	6.55	6.17E-04	5.94	5.70E-05	3.53	9.23E-04	3.08
	160	1.04E-05	3.03	7.61E-05	3.02	7.45E-06	2.93	1.25E-04	2.89
	320	1.32E-06	2.98	9.60E-06	2.99	9.42E-07	2.98	1.56E-05	3.00
H_1 Conserved DG scheme	40	1.03E-02	-	4.67E-02	-	3.27E-04	-	3.97E-03	-
	80	9.88E-05	6.70	6.97E-04	6.07	3.41E-05	3.26	5.81E-04	2.77
	160	1.16E-05	3.09	8.26E-05	3.08	4.23E-06	3.01	7.94E-05	2.87
	320	1.43E-06	3.02	1.02E-05	3.01	5.29E-07	3.00	1.01E-05	2.97
Integration DG scheme	40	1.77E-05	-	1.94E-04	-	2.32E-04	-	2.80E-03	-
	80	9.16E-07	4.27	1.75E-05	3.48	2.92E-05	2.99	4.59E-04	2.61
	160	5.41E-08	4.08	1.17E-06	3.90	3.70E-06	2.98	6.07E-05	2.92
	320	3.33E-09	4.02	7.45E-08	3.98	4.65E-07	2.99	7.72E-06	2.98

Table 4.6

Example 4.2, 1-soliton solution of the CD system (2.2): nonuniform meshes ($2dx, dx, 2dx, dx \dots$) in the computational domain $[-10, 10]$, P^2 elements, at time $T = 1$. The parameters $p_1 = 1.0, \alpha_1 = 4.0$.

	N	$\ u - u_h\ _{L^2}$	Order	$\ u - u_h\ _{L^\infty}$	Order	$\ \rho - \rho_h\ _{L^2}$	Order	$\ \rho - \rho_h\ _{L^\infty}$	Order
H_0	40	9.14E-04	–	4.84E-03	–	1.48E-03	–	2.05E-02	–
	80	1.14E-04	3.01	1.51E-03	1.68	4.17E-04	1.83	5.79E-03	1.83
	160	2.77E-05	2.04	3.65E-04	2.05	1.06E-04	1.97	1.53E-03	1.92
	DG scheme	320	6.88E-06	2.01	9.14E-05	2.00	2.68E-05	1.99	4.08E-04
H_1	40	2.85E-04	–	4.98E-03	–	5.94E-04	–	7.86E-03	–
	80	3.43E-05	3.05	6.53E-04	2.93	7.00E-05	3.08	1.05E-03	2.90
	160	4.30E-06	3.00	8.63E-05	2.92	8.86E-06	2.98	1.41E-04	2.91
	DG scheme	320	5.38E-07	3.00	1.09E-05	2.98	1.11E-06	2.99	1.79E-05

$$\begin{cases} u = \frac{g}{f}, \\ x = x(y_0, s) + \int_{y_0}^y \rho(\zeta, s) d\zeta = y - 2(\ln f)_s, \quad t = s, \end{cases} \quad (4.2)$$

$$f = \begin{vmatrix} A_I & I \\ -I & B_I \end{vmatrix}, \quad g = \begin{vmatrix} A_I & I & \mathbf{e}^T \\ -I & B_I & \mathbf{0}^T \\ \mathbf{0} & -\alpha^T & 0 \end{vmatrix}$$

where $A_I, B_I, I \in \mathbb{R}^{m \times m}$, m is integer denoting the number of soliton, and I is an identity matrix, $\mathbf{0}, \mathbf{e}, \alpha \in \mathbb{R}^m$ are m -component row vectors whose elements are defined, respectively, by

$$a_{ij} = \frac{1}{2(\frac{1}{p_i} + \frac{1}{p_j})} e^{\xi_i + \xi_j}, \quad b_{ij} = \frac{\alpha_i \alpha_j}{2(\frac{1}{p_i} + \frac{1}{p_j})}, \quad (4.3)$$

$$\mathbf{e} = (e^{\xi_1}, e^{\xi_2}, \dots, e^{\xi_m}), \quad \alpha = (\alpha_1, \alpha_2, \dots, \alpha_m), \quad \text{with } \xi_i = p_i y + \frac{s}{p_i} + y_{i0}, \quad i = 1, 2, \dots, m.$$

We fix the constant of integration in x by choosing $y_0 = y_L$, and $p_i, \alpha_i, y_{i0} \in \mathbb{C}$ are constants.

The L^2, L^∞ error order of 1-soliton solution for CD system are calculated numerically and reported in Table 4.5. We compare four kinds of DG schemes at time $T = 10$ with uniform meshes in $[-10, 10]$. The H_0 dissipative DG numerical scheme with $\alpha = 0.1, \beta = 0, \mu = 0.5$ in (2.16) can reach the optimal $(k+1)$ -th order of accuracy for u and ρ , so can H_1 conserved DG scheme. And the integration DG scheme has the optimal $(k+2)$ -th order of accuracy for u . Notably, the H_0 conserved DG scheme can only reach the optimal error order when k is even, but the suboptimal k -th order of accuracy when k is odd.

Referring to [9], we provide the convergence rate on nonuniform meshes in Table 4.6. Similarly, for the H_0 conserved DG scheme, nonuniform meshes cause the suboptimal order of accuracy on variable u, ρ for all k . However, due to the choice of numerical flux in (2.25), the H_1 conserved DG scheme can achieve the optimal order of accuracy on variable u, ρ with nonuniform meshes regardless of the parity of k .

For the same order of accuracy, we notice that H_0 dissipative DG scheme is less accurate than other three schemes. For variable ρ , H_1 conserved DG scheme is more accurate than H_0 conserved DG scheme, and there is little difference for variable u . In these four schemes, the integration DG scheme is most accurate one.

Table 4.7

Example 4.2, the time evolution of conserved quantities for 1-soliton solution for the CD system (2.2), with computational domain $[-20, 20]$ and $N = 160$ cells at time $T = 10$.

p^k	H_0 conserved DG scheme		H_1 conserved DG scheme		Integration DG scheme	
	ΔH_0	ΔH_1	ΔH_0	ΔH_1	ΔH_0	ΔH_1
p^2	1.96E-06	2.96E-06	1.94E-06	1.23E-07	4.38E-07	1.24E-07
p^3	1.51E-07	1.16E-08	4.92E-08	2.18E-08	7.61E-08	5.88E-08

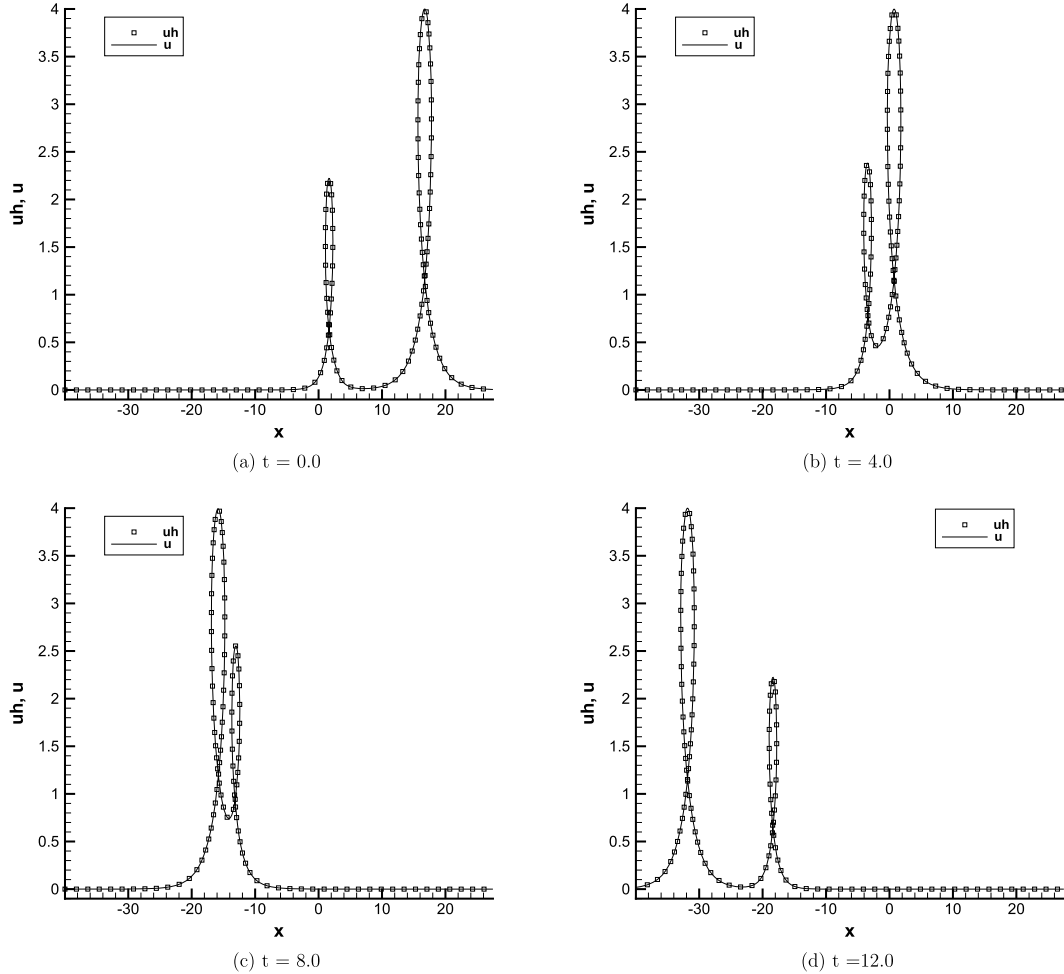


Fig. 4.2. Example 4.2, two-loop-soliton solution of the short pulse equation (2.1): H_0 conserved DG scheme with $N = 160$ cells, P^2 elements. The parameters $\alpha_1 = e^{-2}$, $\alpha_2 = e^{-8}$, $p_1 = 0.9$, $p_2 = 0.5$.

The changes of quantity H_0 and H_1 with time are contained in Table 4.7. The quantities ΔH_0 , ΔH_1 are defined as

$$\Delta H_0 = \sum_{j=1}^{N+1} \left| \left(\int_{I_j} \rho_h u_h^2 \Big|_{t=T} dy - \int_{I_j} \rho_0 u_0^2 dy \right) \right|,$$

$$\Delta H_1 = \sum_{j=1}^{N+1} \left| \left(\int_{I_j} \rho_h^2 + \omega_h^2 \Big|_{t=T} dy - \int_{I_j} \rho_0^2 + \omega_0^2 dy \right) \right|,$$

where ρ_0, u_0, ω_0 are the initial conditions. Even though the fully discrete schemes may not be conservative, the two conserved quantities change slightly. To reduce the fluctuation of H_0 and H_1 , we can increase the accuracy of temporal and spatial discretizations.

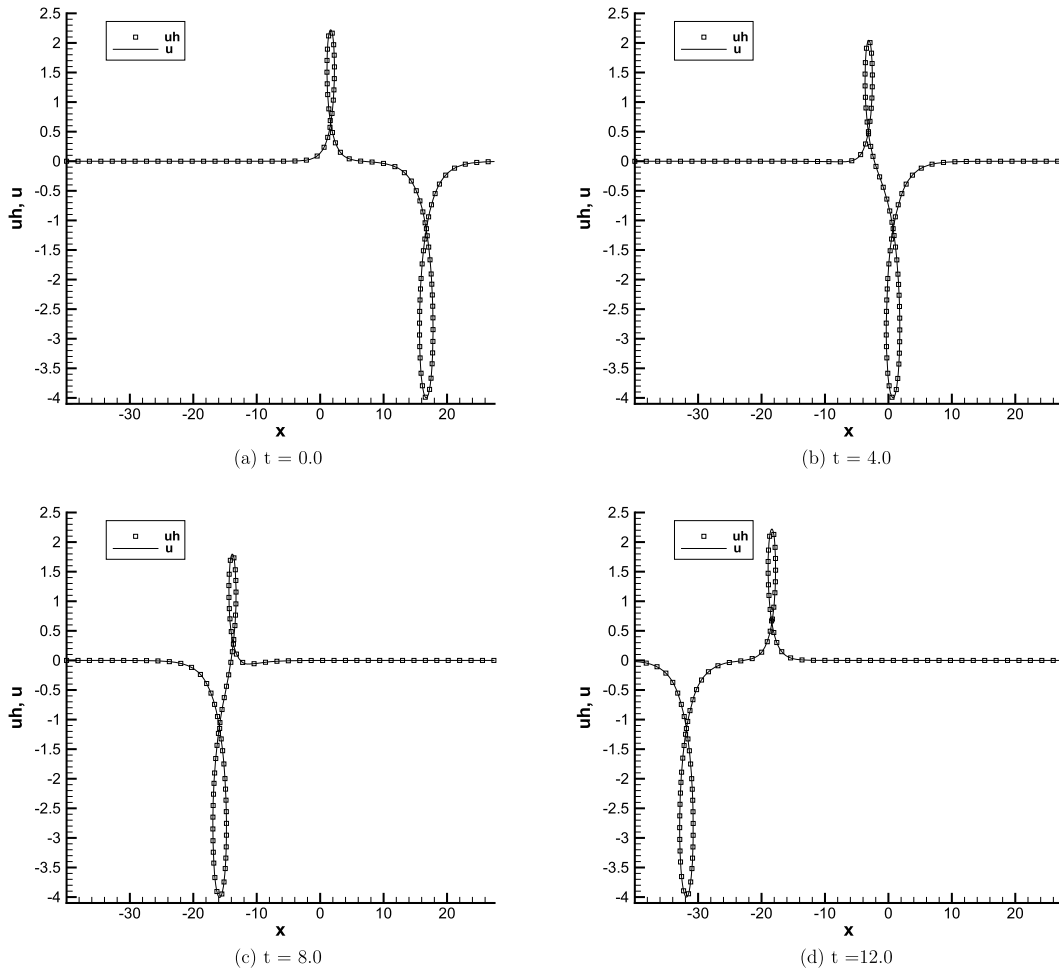


Fig. 4.3. Example 4.2, loop-antiloop-soliton solution of the short pulse equation (2.1): H_1 conserved DG scheme with $N = 160$ cells, P^2 elements. The parameters $\alpha_1 = e^{-2}$, $\alpha_2 = -e^{-8}$, $p_1 = 0.9$, $p_2 = 0.5$.

Next we show the capability of these DG schemes to simulate the singular soliton solutions. For the 2-soliton solution of the corresponding CD system, according to the choice of parameters, the solutions of the short pulse equation (2.1) can be divided into three classes: two-loop-soliton solution in Fig. 4.2, loop-antiloop-soliton solution in Fig. 4.3, two smooth-soliton solution (so called breather solution) in Fig. 4.4. The DG schemes conduct accurate approximations for these soliton solutions.

Example 4.3. In this example, we consider the complex short pulse equation

$$u_{xt} = u + \frac{1}{2}(|u|^2 u_x)_x, \quad u \in \mathbb{C} \quad (4.4)$$

which is linked with the complex CD system (3.4). The exact solution can be also expressed as the determinant form (4.2), the elements of A_I and B_I are distinct from Example 4.2 in (4.3):

$$a_{ij} = \frac{1}{2(\frac{1}{p_i} + \frac{1}{p_j^*})} e^{\xi_i + \xi_j^*}, \quad b_{ij} = \frac{\alpha_i^* \alpha_j}{2(\frac{1}{p_i^*} + \frac{1}{p_j})}.$$

$$\text{with } \xi_i = p_i y + \frac{s}{p_i} + y_{i0}, \quad \xi_i^* = p_i^* y + \frac{s}{p_i^*} + y_{i0}^*, \quad i = 1, 2, \dots, m,$$

where $*$ denotes the complex conjugate, and $p_i, \alpha_i, y_{i0} \in \mathbb{C}$ are constants. The shape of solution depends on the choice of parameters $p_i, i = 1, 2, \dots, m$. For 2-soliton solution, if $p_1 = p_2 \in \mathbb{C}$, then it degenerates to 1-soliton solution. Otherwise, it has two solitons. We first take the parameters as $p_1 = 0.5 + i$, $p_2 = 0.8 + 2i$, i.e. two smooth-soliton, so called breather solution. We plot the moduli $|u|$ and $|u_h|$ at $T = 0, 25, 35, 60$ in Fig. 4.5. The computational domain is $[-50, 50]$ with

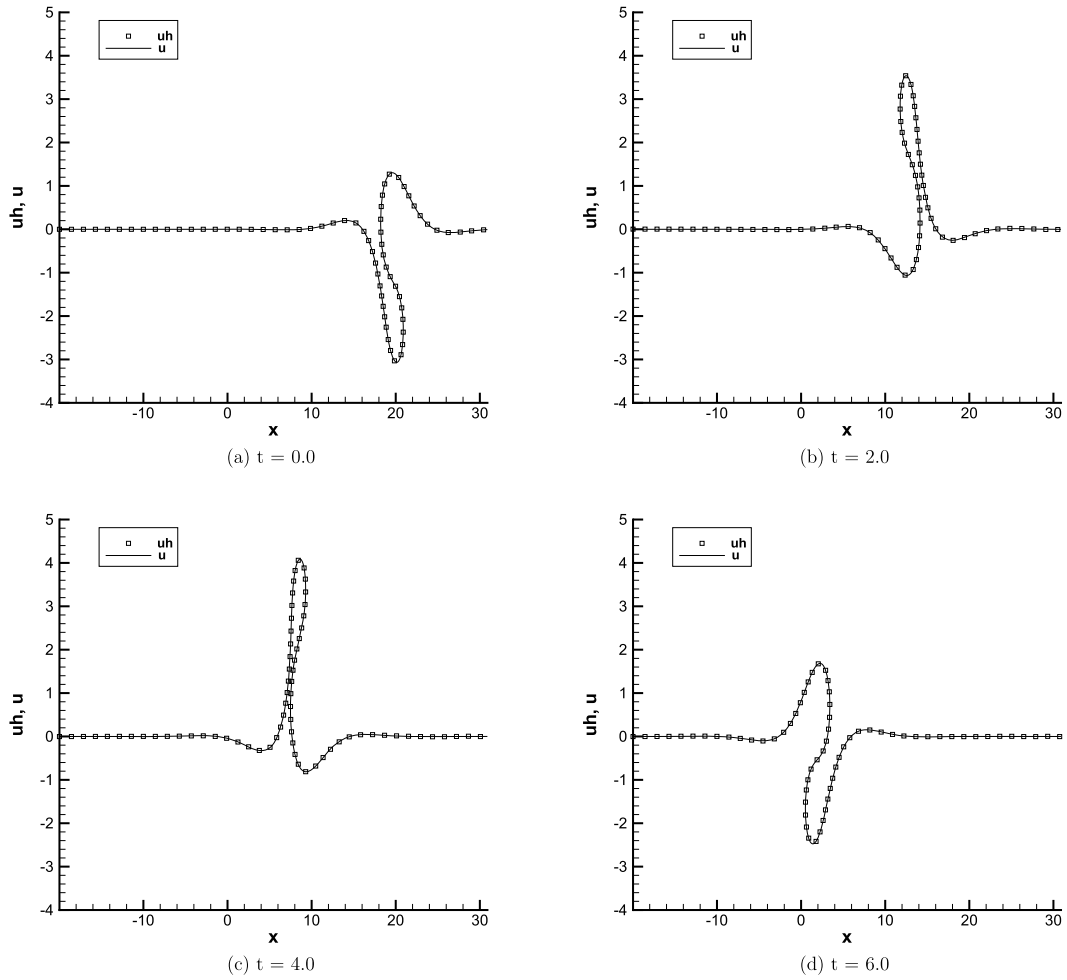


Fig. 4.4. Example 4.2, breather solution of the short pulse equation (2.1): Integration DG scheme with $N = 160$ cells, P^2 elements. The parameters $\alpha_1 = e^{-8}(1+i)$, $\alpha_2 = e^{-8}(1-i)$, $p_1 = 0.4 + 0.44i$, $p_2 = 0.4 - 0.44i$.

Table 4.8

Example 4.3, the time evolution of conserved quantities for breather solution of the complex CD system (3.4), with the computational domain $[-50, 50]$ and $N = 320$ cells at time $T = 10$. The parameters $\alpha_1 = e^{-6}$, $\alpha_2 = e^4$, $p_1 = 0.5 + i$, $p_2 = 0.8 + 2i$.

p^k	H_0 conserved DG scheme		H_1 conserved DG scheme		Integration DG scheme	
	ΔH_0	ΔH_1	ΔH_0	ΔH_1	ΔH_0	ΔH_1
p^1	2.43E-02	1.67E-01	1.28E-02	9.15E-08	2.05E-04	3.25E-09
p^2	3.56E-06	1.63E-06	3.70E-06	3.29E-09	5.64E-07	7.68E-10
p^3	1.04E-07	2.19E-07	6.98E-08	7.70E-10	1.28E-09	9.93E-12

uniform meshes $N = 320$. In Fig. 4.6, an interaction of loop-soliton and cuspon-soliton is shown in domain $[-20, 20]$ and parameters $p_1 = 0.9 + 0.5i$, $p_2 = 2.0 + 2i$. We can see clearly that the moving soliton interaction is resolved very well comparing with [12].

Similar to the short pulse equation (2.1), the conserved quantities H_0 , H_1 of the complex CD system (3.4) are contained in Table 4.8. Increasing the degree k of piecewise polynomial space can reduce the change of conserved quantities. The fluctuations of ΔH_0 , ΔH_1 for integration DG scheme is the most slight among these three DG methods.

Example 4.4. The complex form of coupled short pulse equations

$$\begin{cases} u_{xt} = u + \frac{1}{2}((|u|^2 + |v|^2)u_x)_x, \\ v_{xt} = v + \frac{1}{2}((|v|^2 + |u|^2)v_x)_x, \end{cases} \quad u, v \in \mathbb{C} \quad (4.5)$$

is integrable and admits N -soliton solution. The corresponding CD system (3.6) with the exact solutions was developed in [14]. Here, we perform the simulation of 2-smooth-soliton solution at time $T = 0, 25, 45, 65$, in which the collision is elastic

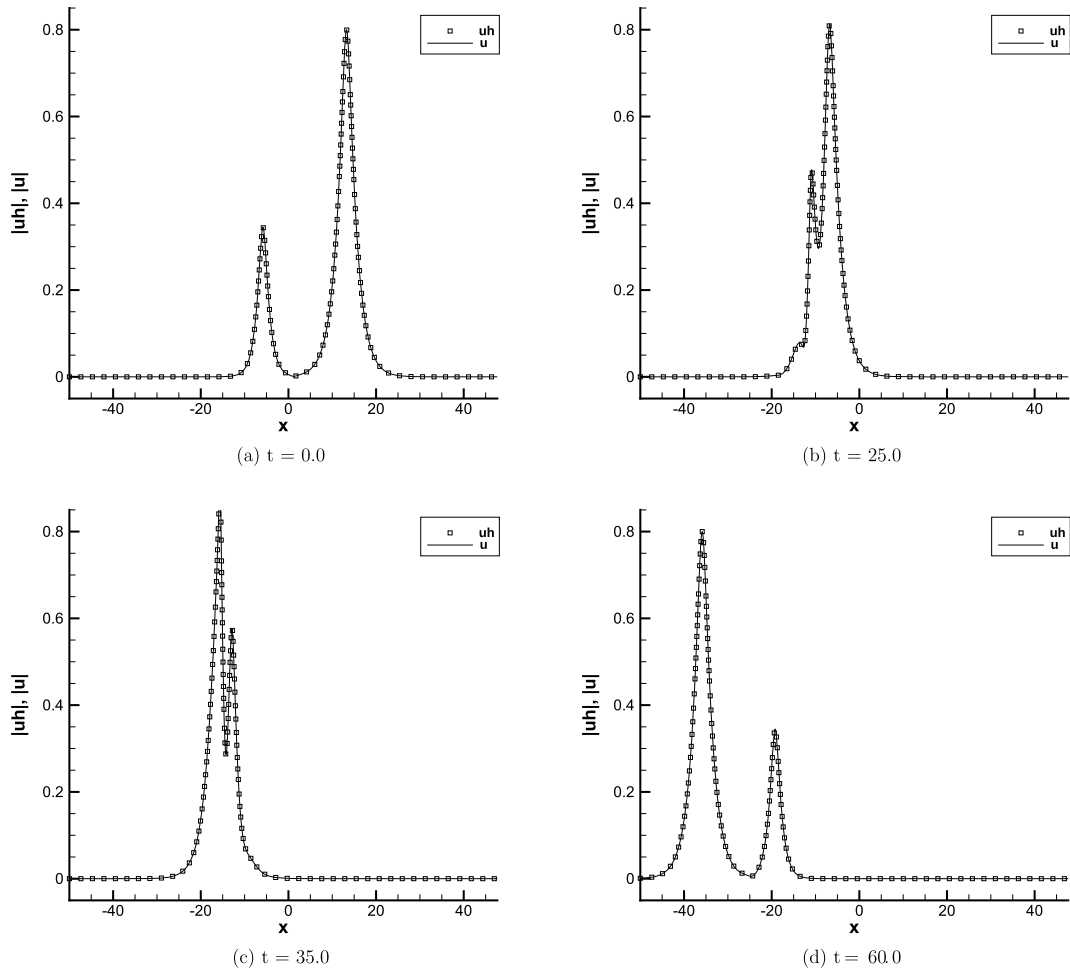


Fig. 4.5. Example 4.3, breather solution for the complex short pulse equation (4.4): H_1 conserved DG scheme with $N = 320$ cells, P^2 elements. The parameters $\alpha_1 = e^{-6}$, $\alpha_2 = e^4$, $p_1 = 0.5 + i$, $p_2 = 0.8 + 2i$.

as shown in Fig. 4.7. Compared with the results in [14], all DG schemes resolve the collision well. Hence, we only show the result of H_0 conserved DG scheme in Fig. 4.7.

Example 4.5. In this example, we give a 1-cuspon-soliton solution for the coupled modified short pulse equation

$$u_{xt} = u + \frac{1}{2}v(u^2)_{xx}, \quad v_{xt} = v + \frac{1}{2}u(v^2)_{xx}, \quad u, v \in \mathbb{R} \quad (4.6)$$

in the form of

$$\begin{cases} u = \frac{g_1}{f}, \quad v = \frac{g_2}{f}, \\ x = y - (\ln f)_s, \quad t = s. \end{cases}$$

The τ -functions f, g_1, g_2 are

$$f = 1 + \frac{a_1 b_1 p_1^2}{4} e^{2\xi_1}, \quad g_1 = a_1 e^{\xi_1}, \quad g_2 = b_1 e^{\xi_1},$$

$$\xi_1 = p_1 y + \frac{s}{p_1} + \xi_{10},$$

where a_1, b_1, p_1, ξ_{10} are real constants. The numerical solution u_h simulated by H_1 conserved DG scheme is shown in Fig. 4.8. The other two schemes, the H_0 conserved scheme and the integration DG scheme perform very similar to the H_1 conserved DG scheme. The solution v_h is also a cuspon-soliton solution whose shape is just like u_h .

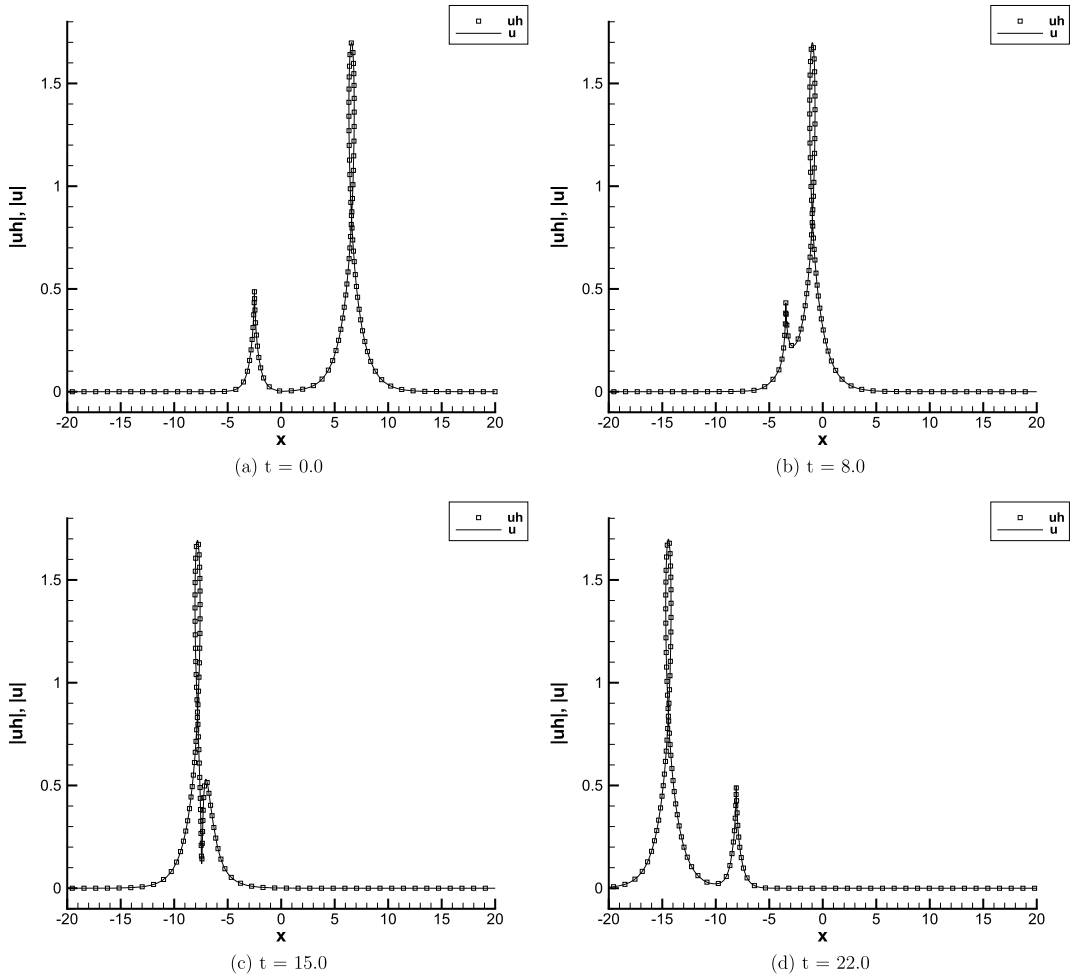


Fig. 4.6. Example 4.3, loop-cuspon-soliton solution for the complex short pulse equation (4.4): H_1 conserved DG scheme with $N = 320$ cells, P^2 elements. The parameters $\alpha_1 = e^{-6}$, $\alpha_2 = e^4$, $p_1 = 0.9 + 0.5i$, $p_2 = 2.0 + 2i$.

Example 4.6. In this example, we consider the complex modified short pulse equation of defocusing type

$$u_{xt} = u - \frac{1}{2}u^*(u^2)_{xx}, \quad u \in \mathbb{C}, \quad (4.7)$$

and its corresponding CD system (3.12) has solution:

$$\begin{cases} u = \frac{1}{2} \frac{g}{f} e^{i(\kappa y + \gamma s)}, \\ x = -\kappa \gamma y + \frac{1}{4}s - (\ln f)_s, \end{cases}$$

where

$$f = 1 + e^\xi, \quad g = 1 + e^{\xi - 2i\varphi}, \\ \xi = \beta y + \omega s, \quad \omega = -\sin \varphi, \quad \beta = \frac{-\kappa \sin \varphi}{\cos \varphi - \gamma}.$$

In Fig. 4.9, we can resolve the dark cuspon-soliton solution as well as the breather solution. Our numerical schemes are also applied for the bright soliton solutions of the focusing type short pulse equation [15,16] with zero or nonzero boundary, we just omit the duplicate numerical tests.

4.3. Solve the short pulse type equations by transforming it to the sine-Gordon equations

Example 4.7. In this example, we test the DG schemes for the sine-Gordon equation

$$z_{ys} = \sin z, \quad (4.8)$$

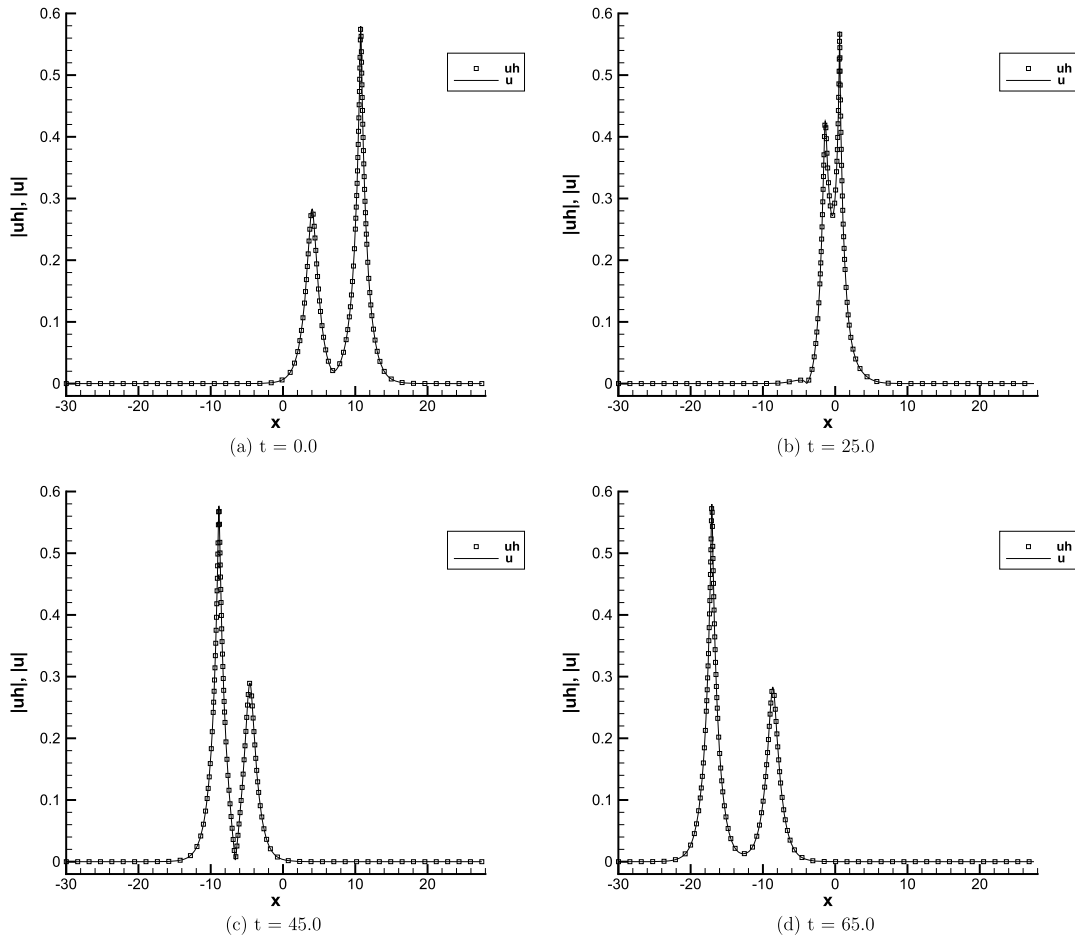


Fig. 4.7. Example 4.4, two smooth-soliton solution of the coupled short pulse equation in complex form (4.5): H_0 conserved DG scheme with $N = 320$ cells, p^2 elements.

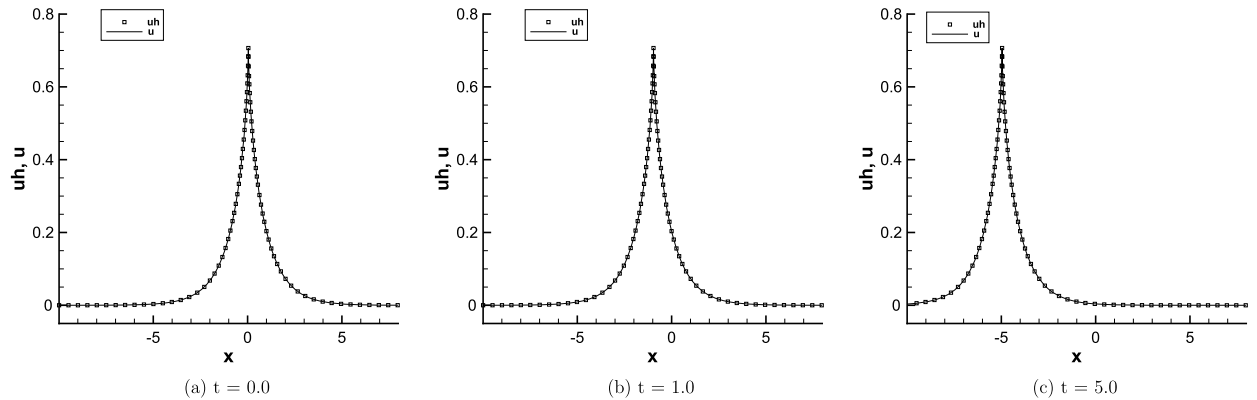


Fig. 4.8. Example 4.5, 1-cuspon-soliton solution u of the coupled modified short pulse equation (4.6): H_1 conserved DG scheme with $N = 160$ cells, p^2 elements. The parameters $p_1 = 1.0$, $a_1 = 0.5$, $b_1 = 1.0$.

with the 1-soliton solution:

$$z(y, s) = 4 \arctan(\exp(y + s)). \quad (4.9)$$

In Table 4.9, we give the errors and convergence rates of two DG schemes. The DG scheme (2.41) can reach optimal $(k+1)$ -th order of accuracy. And the integration DG scheme (2.42) can also achieve the optimal order of accuracy, which is $(k+2)$ -th order for u_h .

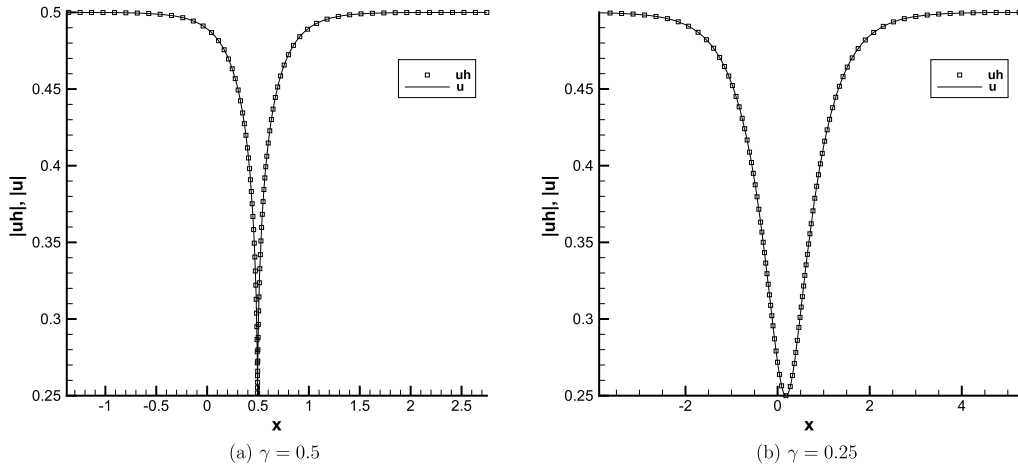


Fig. 4.9. Example 4.6, two types solution of the defocusing complex modified short pulse equation (4.7): H_0 conserved DG scheme with $N = 160$ cells, p^2 elements, at time $T = 1$. The parameters $\kappa = 1.0$, $\varphi = \frac{2}{3}\pi$.

Table 4.9

Example 4.7, 1-soliton solution (4.9) of the sine-Gordon equation (4.8): The computational domain $[-5, 5]$, at time $T = 1$.

	N	DG scheme (2.41)				Integration DG scheme (2.42)			
		$\ z - z_h\ _{L^2}$	Order	$\ z - z_h\ _{L^\infty}$	Order	$\ z - z_h\ _{L^2}$	Order	$\ z - z_h\ _{L^\infty}$	Order
p^1	40	1.95E-03	–	2.56E-02	–	1.53E-04	–	1.65E-03	–
	80	4.90E-04	1.99	7.17E-03	1.83	1.94E-05	2.99	2.28E-04	2.85
	160	1.23E-04	2.00	1.84E-03	1.96	2.43E-06	3.00	2.98E-05	2.94
	320	3.07E-05	2.00	4.64E-04	1.99	3.04E-07	3.00	3.78E-06	2.98
p^2	40	1.41E-04	3.21	1.32E-03	3.09	7.91E-06	4.22	7.96E-05	4.15
	80	1.77E-05	2.99	1.84E-04	2.84	4.99E-07	3.99	5.61E-06	3.83
	160	2.22E-06	3.00	2.37E-05	2.96	3.13E-08	4.00	3.62E-07	3.95
	320	2.77E-07	3.00	2.99E-06	2.99	1.96E-09	4.00	2.28E-08	3.99

Table 4.10

Example 4.7, the time evolution of conserved quantity H_2 for 1-soliton solution (4.9) for the sine-Gordon equation (4.8), with the computational domain $[-30, 30]$ and $N = 320$ cells at time $T = 10$.

ΔH_2	DG scheme (2.41)	Integration DG scheme (2.42)
p^1	6.39E-03	6.85E-07
p^2	7.12E-06	4.93E-10
p^3	7.75E-09	4.90E-10

We define

$$\Delta H_2 = \sum_{j=1}^{N+1} \left(\int_{I_j} \omega_h^2 \Big|_{t=T} dy - \int_{I_j} \omega_0^2 dy \right)$$

where ω_h is defined in (2.41c). Compared with DG scheme (2.41), the fluctuation of H_2 in integration DG scheme is very slight, as shown in Table 4.10.

In [29], two-loops-soliton, loop-antiloop-soliton and breather solutions can be found for the short pulse equation (2.1). We use these solutions to validate our numerical schemes. We plot figures of the antiloop-loop and breather solutions for the short pulse equation (2.1) in Fig. 4.10, 4.11. For those two cases, the initial data of the sine-Gordon equation is required to be continuous. Thus we can get the temporal and spatial derivatives z_s, z_y of z . The initial condition for the two-loop-soliton solution is discontinuous, therefore, we give the initial derivatives piecewisely. The integration DG scheme obtains the accurate solution as shown in Fig. 4.12. These three kinds of solutions can be resolved well compared with the exact solutions in [29].

Example 4.8. We consider the novel coupled short pulse system

$$\left. \begin{aligned} u_{xt} &= u + \frac{1}{6}(u^3)_{xx} + \frac{1}{2}v^2u_{xx}, \\ v_{xt} &= v + \frac{1}{6}(v^3)_{xx} + \frac{1}{2}u^2v_{xx}, \end{aligned} \right\} u, v \in \mathbb{R} \quad (4.10)$$

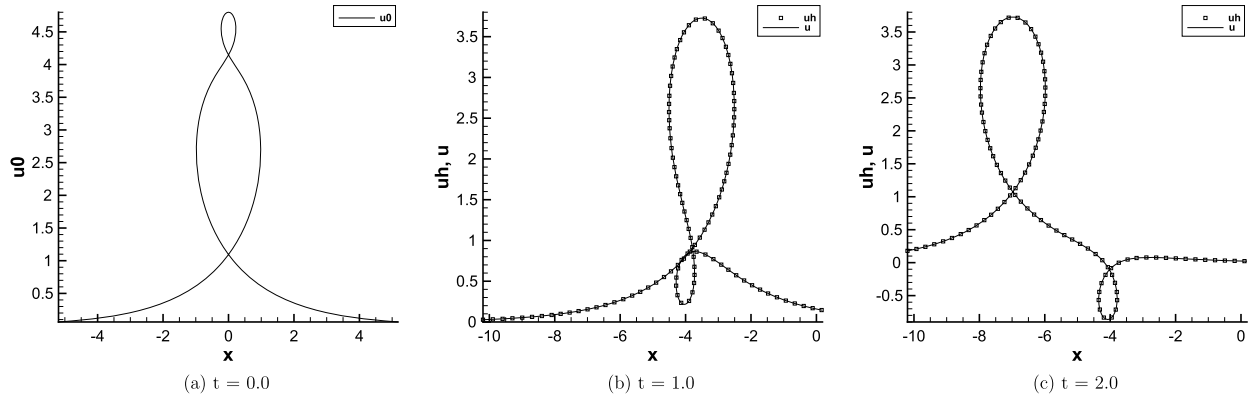


Fig. 4.10. Example 4.7, antiloop-loop-soliton solution of the short pulse equation (2.1): Integration DG scheme with $N = 160$ cells, P^2 elements.

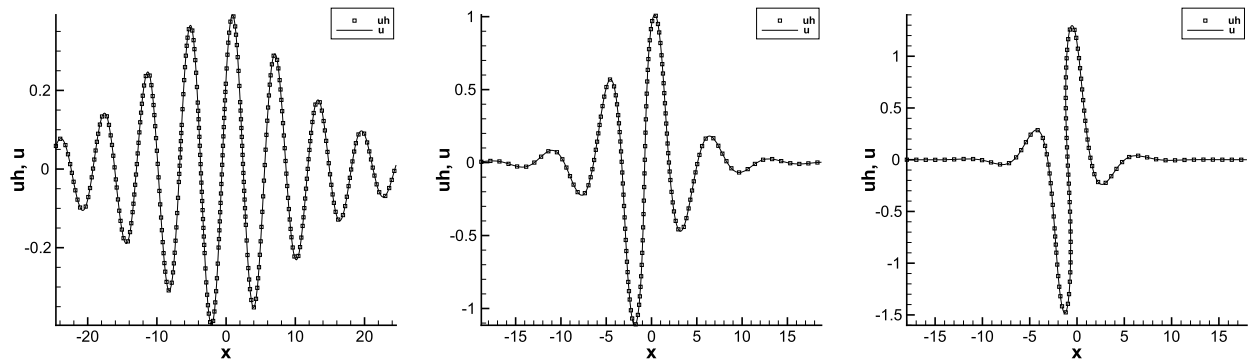


Fig. 4.11. Example 4.7, breather solution of the short pulse equation (2.1): DG scheme (2.41) with $N = 160$ cells, P^2 elements at time $T = 1$.

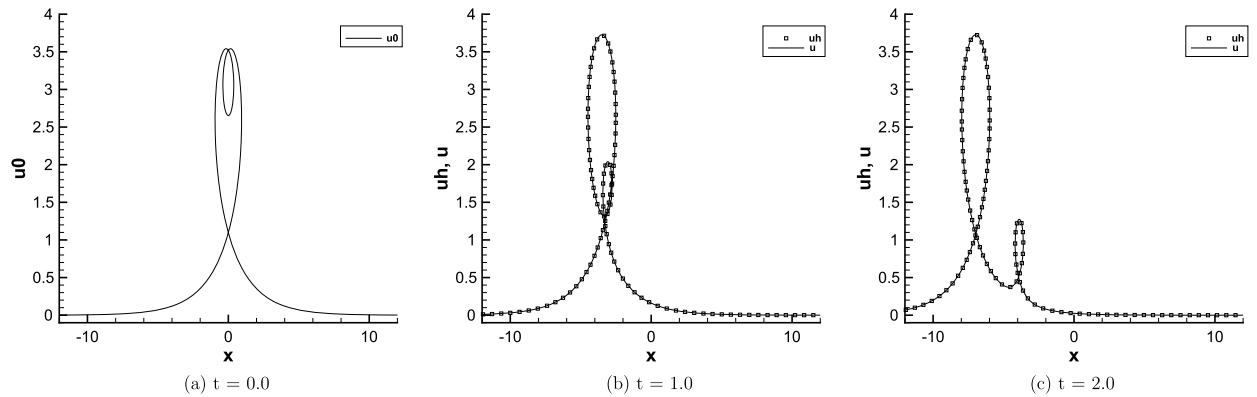


Fig. 4.12. Example 4.7, two-loop-soliton solution of the short pulse equation (2.1): Integration DG scheme with $N = 160$ cells, P^2 elements.

which can only be converted into the sine-Gordon system (3.14) with exact solution

$$z = 2i \ln \frac{f^*}{f}, \quad \tilde{z} = 2i \ln \frac{g^*}{g}.$$

Linking with the hodograph transformation (3.15), we obtain the solution of this novel coupled short pulse system (4.10)

$$\begin{cases} u = \frac{1}{2}(z + \tilde{z})_s = i \left(\ln \left(\frac{f^* g^*}{f g} \right) \right)_s, \\ v = \frac{1}{2}(z - \tilde{z})_s = i \left(\ln \left(\frac{f^* g}{f g^*} \right) \right)_s, \\ x = y - 2(\ln(f f^* g g^*))_s, \quad t = s. \end{cases}$$

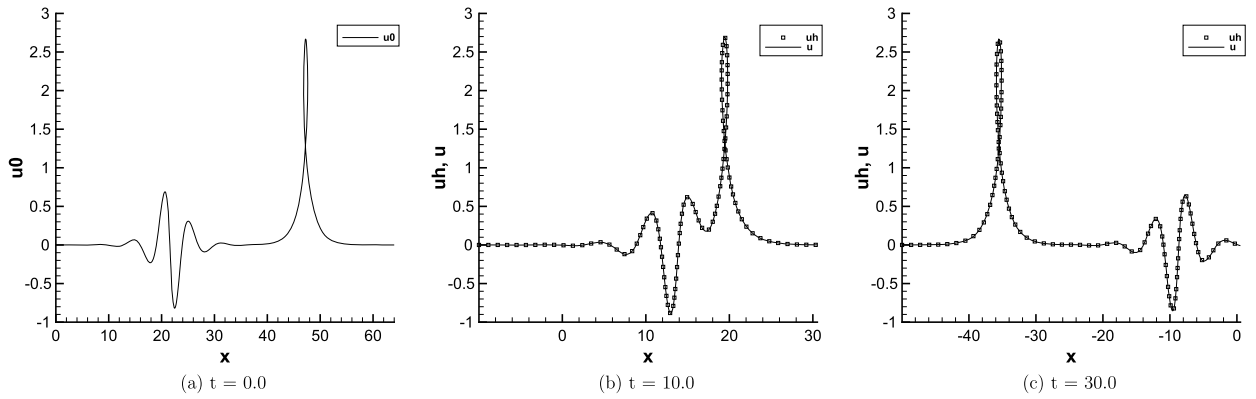


Fig. 4.13. Example 4.8, loop-breather-soliton interaction u of the novel coupled short pulse system (4.10): Integration DG scheme with $N = 160$ cells, p^2 elements.

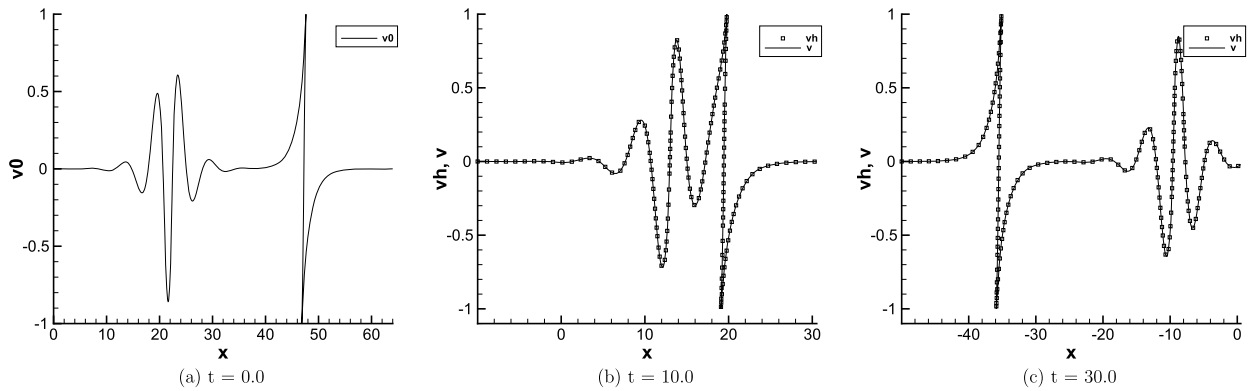


Fig. 4.14. Example 4.8, breather-cuspon-soliton interaction v of the novel coupled short pulse system (4.10): Integration DG scheme with $N = 160$ cells, p^2 elements.

The form of τ functions f, g are listed in [11]. We consider the solution like 3-soliton solution which is a combination of 1-loop-soliton and 2-breather solution. In Fig. 4.13 and 4.14, the process of interaction is displayed by the integration DG scheme, which resolve the collision efficiently.

5. Conclusion

In this paper, we developed DG methods for short pulse type equations. First, we directly proposed the E_0 conserved DG scheme for the short pulse equation for solving smooth solutions. Thereafter for nonclassical solutions such as loop-soliton, cuspon-soliton solutions, we introduced the DG schemes based on the hodograph transformations, which link the short pulse equation with the CD system or the sine-Gordon equation. For the CD system, we constructed the H_0 and H_1 conserved DG schemes, in addition to solving singular solutions, which can preserve the corresponding conserved quantities. Additionally, an integration DG scheme was proposed. Theoretically, we proved the a priori error estimates for the H_1 conserved scheme and the integration DG scheme. More precisely, the optimal order of accuracy in L^2 norm can be proved for the H_1 conserved DG scheme. For the integration DG scheme, the optimal order of accuracy in L^2 norm for two variables can be obtained, but suboptimal order of accuracy in L^∞ norm for the other one. Numerically, on uniform meshes, both the H_1 conserved scheme and the integration DG scheme can achieve the optimal convergence rates in our numerical tests, however, the order of accuracy for the H_0 conserved DG scheme is optimal for the even order piecewise polynomial space and suboptimal in the odd order case. Nonuniform meshes will cause suboptimal order of accuracy for E_0, H_0 conserved DG scheme regardless of the parity of the polynomial degrees. For the sine-Gordon equation, we also proposed two effective DG schemes to solve it in case there is no transformation linking the short pulse equation with the CD system. These DG schemes can be adopted to the relevant generalized short pulse type equations, which have been shown in our numerical tests. Finally, several numerical examples in different circumstances were shown to illustrate the accuracy and capability of these DG schemes.

Declaration of competing interest

The authors declare that they have no known competing financial interests or personal relationships that could have appeared to influence the work reported in this paper.

References

- [1] M. Abramowitz, I.A. Stegun, Handbook of Mathematical Functions, Dover Publications, 1972, 6.
- [2] F. Bassi, S. Rebay, A high-order accurate discontinuous finite element method for the numerical solution of the compressible Navier-Stokes equations, *J. Comput. Phys.* 131 (2) (1997) 267–279.
- [3] J.C. Brunelli, The short pulse hierarchy, *J. Math. Phys.* 46 (12) (2005) 123507.
- [4] J.C. Brunelli, The bi-Hamiltonian structure of the short pulse equation, *Phys. Lett. A* 353 (6) (2006) 475–478.
- [5] S. Brenner, R. Scott, The Mathematical Theory of Finite Element Methods, Springer Science and Business Media, 2007.
- [6] P.G. Ciarlet, The Finite Element Method for Elliptic Problems, North Holland, 1975.
- [7] B. Cockburn, C.-W. Shu, The local discontinuous Galerkin method for time-dependent convection-diffusion systems, *SIAM J. Numer. Anal.* 35 (6) (1998) 2440–2463.
- [8] Y. Chung, C. Jones, T. Schäfer, et al., Ultra-short pulses in linear and nonlinear media, *Nonlinearity* 18 (3) (2005) 1351.
- [9] J. Bona, H. Chen, O. Karakashian, Y. Xing, Conservative, discontinuous Galerkin methods for the generalized Korteweg-de Vries equation, *Math. Comput.* 82 (283) (2013) 1401–1432.
- [10] A. Dimakis, F. Müller-Hoissen, Bidifferential calculus approach to AKNS hierarchies and their solutions, *SIGMA Symmetry Integrability Geom. Methods Appl.* 6 (2010) 55.
- [11] B.F. Feng, An integrable coupled short pulse equation, *J. Phys. A, Math. Theor.* 45 (8) (2012) 085202.
- [12] B.F. Feng, K. Maruno, Y. Ohta, Self-adaptive moving mesh schemes for short pulse type equations and their Lax pairs, *Pac. J. Math. Ind.* 6 (1) (2014) 8.
- [13] B.F. Feng, J. Chen, Y. Chen, et al., Integrable discretizations and self-adaptive moving mesh method for a coupled short pulse equation, *J. Phys. A, Math. Theor.* 48 (38) (2015) 385202.
- [14] B.F. Feng, Complex short pulse and coupled complex short pulse equations, *Phys. D: Nonlinear Phenom.* 297 (2015) 62–75.
- [15] B.F. Feng, L. Ling, Z. Zhu, Defocusing complex short-pulse equation and its multi-dark-soliton solution, *Phys. Rev. E* 93 (5) (2016) 052227.
- [16] B.F. Feng, L. Ling, Z. Zhu, A focusing and defocusing semi-discrete complex short pulse equation and its various soliton solutions, *arXiv preprint, arXiv:1901.02388*, 2019.
- [17] S. Gottlieb, C.-W. Shu, E. Tadmor, Strong stability-preserving high-order time discretization methods, *SIAM Rev.* 43 (1) (2001) 89–112.
- [18] H. Kakuwata, K. Konno Lagrangian, Hamiltonian and Conserved Quantities for Coupled Integrable, Dispersionless Equations, SCAN-9510155, 1995.
- [19] H. Kakuwata, K. Konno, A generalization of coupled integrable, dispersionless system, *J. Phys. Soc. Jpn.* 65 (2) (1996) 340–341.
- [20] O. Karakashian, Y.L. Xing, A posteriori error estimates for conservative local discontinuous Galerkin methods for the generalized Korteweg-de Vries equation, *Commun. Comput. Phys.* 20 (01) (2016) 250–278.
- [21] D. Levy, C.-W. Shu, J. Yan, Local discontinuous Galerkin methods for nonlinear dispersive equations, *J. Comput. Phys.* 196 (2) (2004) 751–772.
- [22] H. Liu, N. Yi, A Hamiltonian preserving discontinuous Galerkin method for the generalized Korteweg-de Vries equation, *J. Comput. Phys.* 321 (2016) 776–796.
- [23] Y. Matsuno, Periodic solutions of the short pulse model equation, *J. Math. Phys.* 49 (7) (2008) 073508.
- [24] Y. Matsuno, A novel multi-component generalization of the short pulse equation and its multisoliton solutions, *J. Math. Phys.* 52 (12) (2011) 123702.
- [25] Y. Matsuno, Integrable multi-component generalization of a modified short pulse equation, *J. Math. Phys.* 57 (11) (2016) 111507.
- [26] W.H. Reed, T.R. Hill, Triangular Mesh Methods for the Neutron Transport Equation, Los Alamos Report LA-UR-73-479, 1973.
- [27] T. Schäfer, C.E. Wayne, Propagation of ultra-short optical pulses in cubic nonlinear media, *Phys. D: Nonlinear Phenom.* 196 (1) (2004) 90–105.
- [28] A. Sakovich, S. Sakovich, The short pulse equation is integrable, *J. Phys. Soc. Jpn.* 74 (1) (2005) 239–241.
- [29] A. Sakovich, S. Sakovich, Solitary wave solutions of the short pulse equation, *J. Phys. A, Math. Gen.* 39 (22) (2006) L361.
- [30] S. Sakovich, Transformation and integrability of a generalized short pulse equation, *Commun. Nonlinear Sci. Numer. Simul.* 39 (2016) 21–28.
- [31] S. Shen, B.F. Feng, Y. Ohta, A modified complex short pulse equation of defocusing type, *J. Nonlinear Math. Phys.* 24 (2) (2017) 195–209.
- [32] S. Sato, K. Oguma, T. Matsuo, et al., A robust numerical integrator for the short pulse equation near criticality, *J. Comput. Appl. Math.* 361 (2019) 343–365.
- [33] H. Wang, C.-W. Shu, Q. Zhang, Stability and error estimates of local discontinuous Galerkin methods with implicit-explicit time-marching for advection-diffusion problems, *SIAM J. Numer. Anal.* 53 (1) (2015) 206–227.
- [34] Y. Xia, Y. Xu, C.-W. Shu, Local discontinuous Galerkin methods for the generalized Zakharov system, *J. Comput. Phys.* 229 (4) (2010) 1238–1259.
- [35] Y. Xia, Y. Xu, A conservative local discontinuous Galerkin method for the Schrödinger-KdV system, *Commun. Comput. Phys.* 15 (4) (2014) 1091–1107.
- [36] Y. Xu, C.-W. Shu, Local discontinuous Galerkin methods for high-order time-dependent partial differential equations, *Commun. Comput. Phys.* 7 (4) (2010) 1–46.
- [37] Y. Xu, C.-W. Shu, Local discontinuous Galerkin methods for three classes of nonlinear wave equations, *J. Comput. Math.* (2004) 250–274.
- [38] Y. Xu, C.-W. Shu, Local discontinuous Galerkin methods for nonlinear Schrödinger equations, *J. Comput. Phys.* 205 (1) (2005) 72–97.
- [39] Y. Xu, C.-W. Shu, Local discontinuous Galerkin methods for two classes of two-dimensional nonlinear wave equations, *Phys. D: Nonlinear Phenom.* 208 (1) (2005) 21–58.
- [40] Y. Xu, C.-W. Shu, Local discontinuous Galerkin methods for the Kuramoto-Sivashinsky equations and the Ito-type coupled KdV equations, *Comput. Methods Appl. Mech. Eng.* 195 (25) (2006) 3430–3447.
- [41] Y. Xu, C.-W. Shu, Dissipative numerical methods for the Hunter-Saxton equation, *J. Comput. Math.* (2010) 606–620.
- [42] J. Yan, C.-W. Shu, A local discontinuous Galerkin method for KdV type equations, *SIAM J. Numer. Anal.* 40 (2) (2002) 769–791.
- [43] J. Yan, C.-W. Shu, Local discontinuous Galerkin methods for partial differential equations with higher order derivatives, *J. Sci. Comput.* 17 (1–4) (2002) 27–47.
- [44] C.H. Yu, B.F. Feng, T.W.H. Sheu, Numerical solutions to a two-component Camassa-Holm equation, *J. Comput. Appl. Math.* 336 (2018) 317–337.
- [45] C. Zhang, Y. Xu, Y. Xia, Local discontinuous Galerkin methods for the μ -Camassa-Holm and μ -Degasperis-Procesi equations, *J. Sci. Comput.* 79 (2019) 1294–1334.
- [46] Q. Zhang, Y. Xia, Conservative and dissipative local discontinuous Galerkin methods for Korteweg-de Vries type equations, *Commun. Comput. Phys.* 25 (2019) 532–563.
- [47] Q. Zhang, Y. Xia, Discontinuous Galerkin methods for the Ostrovsky-Vakhnenko equation, *arXiv:1908.03873 [math.NA]*.